CANCER

Gain-of-function mutations in the catalytic domain of *DOT1L* promote lung cancer malignant phenotypes via the MAPK/ERK signaling pathway

Jiayu Zhang[1,2], Ting Yang[1,2], Mei Han[1,2], Xiaoxuan Wang[1,2], Weiming Yang[1,2], Ning Guo[1,2], Yong Ren[3], Wei Cui[1], Shangxiao Li[4], Yongshan Zhao[4], Xin Zhai[5], Lina Jia[1], Jingyu Yang[1], Chunfu Wu[1], Lihui Wang[1,2]*

Lung cancer is a lethal malignancy lacking effective therapies. Emerging evidence suggests that epigenetic enzyme mutations are closely related to the malignant phenotype of lung cancer. Here, we identified a series of gain-of-function mutations in the histone methyltransferase DOT1L. The strongest of them is R231Q, located in the catalytic DOT domain. R231Q can enhance the substrate binding ability of DOT1L. Moreover, R231Q promotes cell growth and drug resistance of lung cancer cells in vitro and in vivo. Mechanistic studies also revealed that the R231Q mutant specifically activates the MAPK/ERK signaling pathway by enriching H3K79me2 on the *RAF1* promoter and epigenetically regulating the expression of downstream targets. The combination of a DOT1L inhibitor (SGC0946) and a MAPK/ERK axis inhibitor (binimetinib) can effectively reverse the R231Q-induced phenomena. Our results reveal gain-of-function mutations in an epigenetic enzyme and provide promising insights for the precise treatment of lung cancer patients.

INTRODUCTION

Among all malignancies, lung cancer is associated with very high rates of morbidity and mortality across the world (*1*). It is classically divided into two histological types, small cell lung cancer (SCLC) and non–small cell lung cancer (NSCLC) (*2*). SCLC has a low degree of differentiation and a high degree of malignancy, but accounts for a small proportion of cases. Although NSCLC is not as malignant as SCLC, it accounts for about 85% of the total number of lung cancers (*3*, *4*). At present, lung cancer is incurable. The need for new therapeutic strategies provides a compelling reason to elucidate the pathogenic mechanisms, identify the tumor-associated mutations, and search for potential drug targets.

Recent studies have shown that lung cancer tumorigenesis is often accompanied by gene mutations. Loss-of-function mutations, such as mutations that inactivate tumor suppressor genes, are considered as "undruggable." In contrast, therapeutic strategies targeting gain-of-function mutations, such as those that activate oncogenes, are relatively feasible. For example, epidermal growth factor receptor (EGFR) tyrosine kinase inhibitors, which are widely used in lung cancer, have achieved notable therapeutic effects in patients with *EGFR* mutations (*5*). Thus, gain-of-function mutations have attracted more attention. In addition, the evidence suggests that mutations in oncogene functional domains and nearby sites often have a stronger carcinogenic effect. For example, mutations in *EGFR* exons 19, 20, and 21 are more capable of activating downstream cancer-promoting signaling pathways (*6*). Moreover, secondary mutations in these regions, such as the T790M mutation in *EGFR* exon 20, can also confer drug resistance (*7*, *8*). These findings motivate us to discover gain-of-function mutations to understand the pathogenesis of lung cancer and develop precise treatment strategies (*9*, *10*).

Previous reports suggested that abnormal alterations of epigenetic enzymes play critical roles in the occurrence and development of lung cancer (*11*, *12*). Disrupter of telomere silencing 1 like (DOT1L) is the only methyltransferase that regulates methylation of lysine 79 in histone 3 (H3K79me) (*13*, *14*). DOT1L regulates target gene transcription by altering chromatin compaction and is frequently involved in tumor proliferation, self-renewal, invasion, and metastasis (*15*). Clinical studies have shown that DOT1L expression is increased in various malignant tumor tissues, resulting in enhanced methylation, and is closely related to poor prognosis (*16*, *17*). DOT1L participates in the proliferation and self-renewal of cervical cancer cells by activating the WNT signaling pathway (*18*). It also affects the tumor cell cycle and apoptosis by regulating estrogen receptor signaling (*19*), and it can interact with the transcription factor C/EBPβ to mediate multidrug resistance in ovarian cancer cells (*20*). Furthermore, DOT1L is involved in various cancer-related signaling pathways, such as signal transducer and activator of transcription 1 (STAT1) and phosphatidylinositol 3-kinase (PI3K)/AKT (*21*, *22*). There are few reports that DOT1L is associated with the proliferation and epidermal-mesenchymal transition of lung cancer cells (*23*, *24*). The above results provide preliminary evidence that *DOT1L* is an oncogene involved in the development of numerous malignancies.

Because of the recent research focus on regulation of aberrant epigenetic enzymes in cancer, there has been some progress in understanding epigenetic enzyme mutations. Mutation in DNA methyltransferase 3A (DNMT3A) in chronic myelomonocytic leukemia contributes to tumor growth and is associated with poor patient prognosis (*25*). Similarly, mutations in the gene encoding the

[1]Department of Pharmacology, Shenyang Pharmaceutical University, Shenyang 110016, China. [2]Benxi Institute of Pharmaceutical Research, Shenyang Pharmaceutical University, Benxi 117004, China. [3]Department of Pathology, General Hospital of Central Theater Command of People's Liberation Army, Wuhan 430070, China. [4]Department of Biochemistry and Molecular Biology, Shenyang Pharmaceutical University, Shenyang 110016, China. [5]Key Laboratory of Structure-Based Drug Design and Discovery, Ministry of Education, Shenyang Pharmaceutical University, Shenyang 110016, China.
*Corresponding author. Email: lhwang@syphu.edu.cn

histone methyltransferase enhancer of zeste homolog 2 (EZH2) can promote the proliferation of lymphoma and melanoma cells and may serve as potential targets for drug therapy (*26*). Campbell *et al.* (*27*) reported that the mutation rate of *DOT1L* in lung cancer is about 3%. This result, combined with the role of DOT1L in multiple malignancies, prompted us to ask two questions. Are the *DOT1L* mutations in lung cancer also gain-of-function mutations? What is the impact of these mutations on lung cancer? Here, we identified a series of gain-of-function mutations in the *DOT1L* gene. Many of them, including the strongest one, R231Q, are located within the catalytic DOT domain. DOT1L R231Q enriches H3K79me2 on the *RAF1* promoter to remodel the chromatin structure, thereby regulating the expression of genes related to the mitogen-activated protein kinase/extracellular signal–regulated protein kinase (MAPK/ERK) signaling pathway and mediating various malignant phenotypes of lung cancer. In turn, targeting the *DOT1L* R231Q mutation with a DOT1L inhibitor (DOT1Li) and a MAPK/ERK axis inhibitor can effectively reverse the impact of mutation. These findings not only help us to further understand the essential characteristics of lung cancer but also suggest a potential therapeutic approach to lung cancer.

RESULTS

Identification of *DOT1L* expression and mutations in human lung cancer

To explore the role of DOT1L in lung cancer, we interrogated publicly available mRNA data in the Broad Institute Cancer Cell Line Encyclopedia (CCLE) to visualize the expression of *DOT1L* in 1282 tumor cell lines (Fig. 1A). These results showed that *DOT1L* was highly expressed in SCLC and NSCLC. Moreover, we also detected the expression of DOT1L protein in NSCLC from 98 patients. We found that a high level of DOT1L was associated with a bad prognosis (Fig. 1B). The data were confirmed by open access databases, including the PROGgene V2 (GSE30219, GSE11969) database and UALCAN data from The Cancer Genome Atlas (TCGA) (fig. S1, A to C), which indicated that *DOT1L* might play an oncogenic role in lung cancer. Simultaneously, we found that *DOT1L* mutations exist in a variety of tumors. Lung adenocarcinoma and lung squamous cell carcinoma were both among the top 10 cancer types with *DOT1L* mutations. The incidence of *DOT1L* mutations in lung adenocarcinoma was 2.83%, and the incidence in lung squamous cell carcinoma was 1.64% (Fig. 1C). Notably, the TCGA database demonstrated a halved overall survival in lung cancer patients with *DOT1L* mutations (single-nucleotide polymorphisms and small insertions/deletions), suggesting that *DOT1L* mutations may also contribute to poor prognosis in lung cancer patients (Fig. 1D and fig. S1D). Moreover, there was no obvious difference in key clinical characteristics between patients with and without *DOT1L* mutation, including *DOT1L* expression, tumor-node-metastasis (TNM) stage, gender, and age (fig. S1, E and F). This suggests that *DOT1L* mutations are associated with malignant phenotypes of lung cancer, rather than altered *DOT1L* expression, TNM stage, or other factors.

To further elucidate the sites and types of *DOT1L* mutations in lung cancer, we analyzed *DOT1L* mutation cases in NSCLC and SCLC using cBioPortal for Cancer Genomics (*28*). We found that the types of *DOT1L* mutations were missense, truncating, and in-frame mutations (Fig. 1E). In total, 19.6% of all the mutations were missense mutations in the DOT domain. Because DOT1L lacks a SET domain, its catalytic effect on histone methylation relies on its unique DOT domain (*29*). Previous studies have shown that mutations in oncogene functional domains and the adjacent sites often have strong oncogenic potential (*30*, *31*). This suggests that missense mutations in the region of the *DOT1L* gene encoding the DOT domain may be gain-of-function mutations with oncogenic effects.

Multiple mutations in *DOT1L* cause gain-of-function phenotypes

To identify the gain-of-function mutation sites of *DOT1L*, we screened the cBioPortal database and selected the common missense mutations of *DOT1L* in lung cancer. Seven common missense mutations are located in the DOT catalytic domain: E186A, Y216C, S225L, R231Q, I232N, N241T, and F243L. There was also a high-frequency missense mutation site, A1003, outside the DOT domain. A1003 was mutated to both G and S. Using the human NSCLC cell line NCI-H460, we transiently expressed each of the above mutant proteins to investigate the effects of the mutations on the enzymatic activity. We found that cells expressing the DOT1L E186A, S225L, and R231Q mutants had significantly increased levels of H3K79me2 compared to wild type (WT), while cells expressing the I232N mutant tended to reduce levels of H3K79me2 (Fig. 2A). Next, we explored the biological properties of the mutants. The results showed that the cells expressing the DOT1L S225L, R231Q, F243L, and A1003S mutants had an increased capacity for proliferation, while the E186A and I232N mutants had weak proliferation ability (fig. S2, A and B). Migration assays showed that cells expressing the DOT1L Y216C and R231Q mutants migrated faster than WT cells, while cells expressing the A1003S mutant had weak migration ability (fig. S2C). For all the different mutation sites, we combined the data on catalytic activity and biological function (Fig. 2B). The mutations had a spectrum of effects from loss of function to gain of function. On the basis of our assays, the strongest gain-of-function mutation was R231Q in the DOT domain. Cells carrying the R231Q mutation had elevated enzyme activity and increased proliferation and migration capacity. Because we wanted to focus on druggable gain-of-function mutations, we selected R231Q for further analysis.

To evaluate the structural effects of this mutant, we generated structures of DOT1L WT and DOT1L R231Q using PyMOL software and molecular dynamics (MD) simulations (*32*, *33*). Geometric and topological properties of the DOT1L WT and R231Q protein structures, including surface pockets, interior cavities, and cross channels, were determined using CASTp 3.0 software (*34*). We found that the substrate-binding pocket of DOT1L R231Q has a larger surface area and volume than WT DOT1L (Fig. 2C). This indicates that the R231Q mutation would widen the enzyme activity pocket and enhance the substrate binding. Moreover, the occupancy of hydrogen bonds formed at position 231 of the mutant protein was slightly reduced, resulting in a decrease in the rigidity and a relative increase in the flexibility of the R231Q protein, which might also explain why the R231Q mutation causes an enlarged binding pocket (fig. S2D). To test whether the mutations at position 231 to other amino acids are also gain of function, we used the MD simulations to analyze the structure of DOT1L when R231 was replaced with nonpolar amino acids (A, M, W) or polar amino acids (K, N, T) (fig. S2E) (*35*). We found that changing to a nonpolar amino acid at position 231 led to a decrease or no change in the size of the

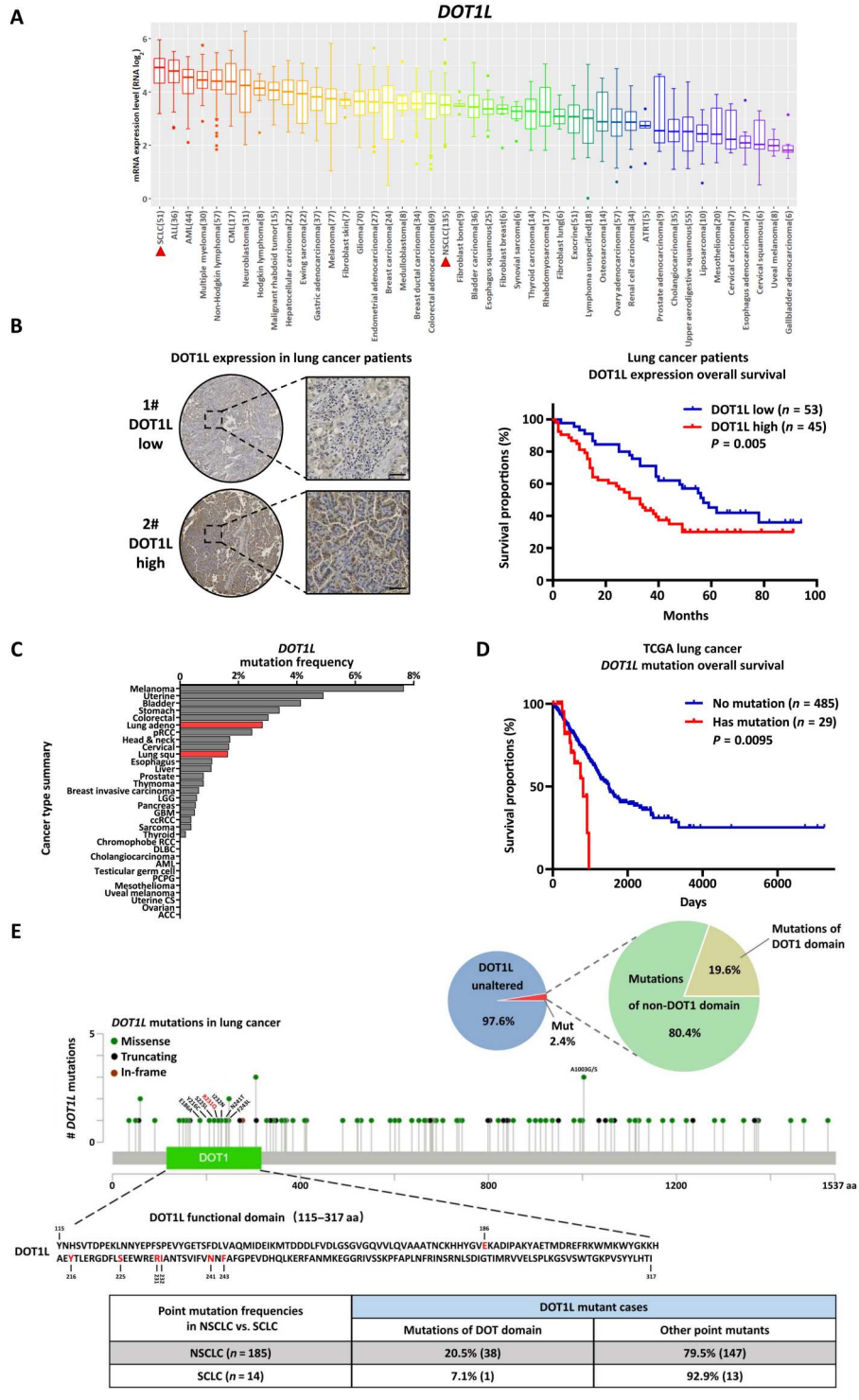

Point mutation frequencies in NSCLC vs. SCLC	DOT1L mutant cases	
	Mutations of DOT domain	Other point mutants
NSCLC (*n* = 185)	20.5% (38)	79.5% (147)
SCLC (*n* = 14)	7.1% (1)	92.9% (13)

Fig. 1. Identification of *DOT1L* expression and mutations in human lung cancer. (**A**) *DOT1L* mRNA expression levels in 1282 human cancer cell lines. *DOT1L* mRNA is highly expressed in SCLC cell lines ($n = 51$) and NSCLC cell lines ($n = 135$), indicated by red triangles. (**B**) Representative sections of NSCLC tumor tissues from two patients showing immunohistochemical detection of DOT1L protein (patient #1 has low DOT1L expression, and patient #2 has high DOT1L expression). Scale bars, 50 μm. The correlation between DOT1L protein expression level and overall survival is also shown. Log-rank (Mantel-Cox) test, $^{**}P < 0.01$. (**C**) Incidence of *DOT1L* mutations in 32 types of cancer, including lung adenocarcinoma (2.83%) and lung squamous cell carcinoma (1.64%). (**D**) Survival probability of lung cancer patients with *DOT1L* mutation ($n = 29$) versus no *DOT1L* mutation ($n = 485$). Log-rank (Mantel-Cox) test, $^{**}P < 0.01$. (**E**) Analysis of mutation frequency and mutation site of *DOT1L* in lung cancer cases from the cBioPortal database.

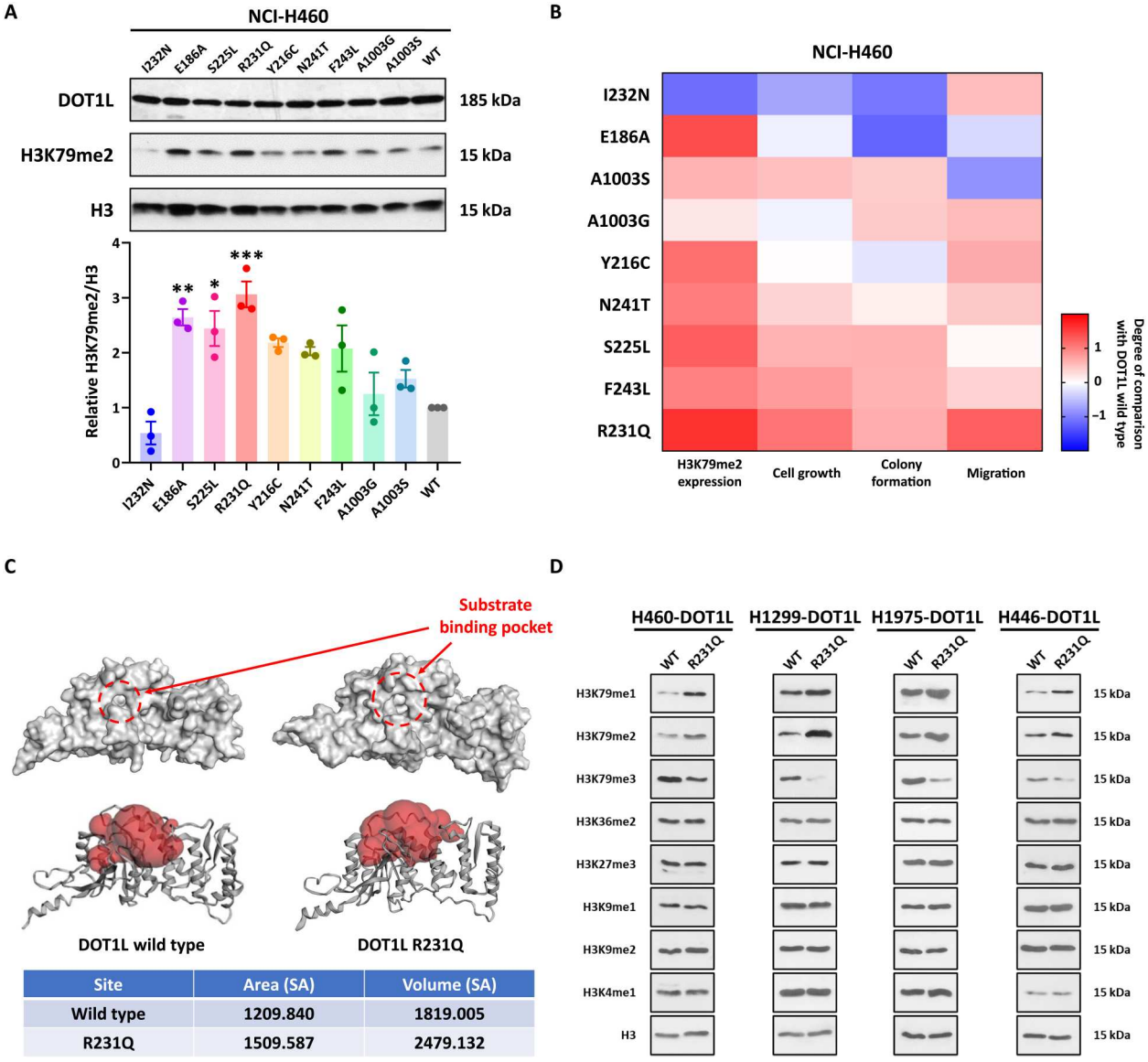

Fig. 2. The enzyme activities and biological functions of lung cancer–associated DOT1L mutants. (**A**) Protein expression levels of H3K79me2 in NCI-H460 cells transiently transfected with recombinant plasmids expressing different DOT1L mutants (E186A, Y216C, S225L, R231Q, I232N, N241T, F243L, A1003G, and A1003S) or WT DOT1L. Data are shown as means ± SEM. *$P < 0.05$, **$P < 0.01$, and ***$P < 0.001$. P values were determined using one-way ANOVA with Tukey's multiple comparisons test. (**B**) Heatmap showing the level of H3K79me2, cell growth, colony formation ability, and migration ability in NCI-H460 cells transiently transfected with recombinant plasmids expressing DOT1L mutants (E186A, Y216C, S225L, R231Q, I232N, N241T, F243L, A1003G, and A1003S) or WT DOT1L. Values are indicated as $\log_2$ fold change. (**C**) Geometric and topological properties of DOT1L WT and R231Q protein structures determined by CASTp 3.0 software. The red shaded areas in the bottom panels are substrate binding pockets. (**D**) Levels of common histone H3 modifications (H3K79me1, H3K79me2, H3K79me3, H3K36me2, H3K27me3, H3K9me1, H3K9me2, and H3K4me1) in DOT1L WT cells or R231Q mutant cells (expressing DOT1L catalytic domain).

substrate binding pocket and the activity of DOT1L. In contrast, polar amino acids enhanced the binding pocket and enzymatic activity, which might be related to the properties of the amino acids. Among all the changes, R231Q increases the surface area and volume of the substrate binding pocket the most.

To fully understand the *DOT1L* R231Q mutation, we selected four cell lines with different *DOT1L* expression levels, including three NSCLC cell lines (NCI-H460 with low *DOT1L*, NCI-H1299 with middle *DOT1L*, and NCI-H1975 with middle *DOT1L*) and one SCLC cell line (NCI-H446 with high *DOT1L*) (fig. S3, A and B), and established stably overexpressing the catalytic domain (amino acids 1 to 416) of WT and mutant DOT1L in these cell lines (H460/H1299/H1975/H446-DOT1L-WT/R231Q) (*13*, *32*). The overexpression levels of *DOT1L* were confirmed to be within the pathophysiological range of lung cancer (fig. S3, C to E). Next, we verified the methylation status of histone H3 in the cells to demonstrate the catalytic activity of the enzymes. Studies have shown that H3K79me1 and H3K79me2 can relax chromatin to promote target gene transcription (*36*, *37*), while H3K79me3 is thought to lead to repression of target gene transcription (*38*). In

cells expressing DOT1L R231Q, we found that the levels of H3K79me1 and H3K79me2 were increased, while the level of H3K79me3 was decreased. In addition, we also analyzed other methylation changes, including H3K4me1 and H3K36me2, which are associated with transcriptional activation, and H3K9me1, H3K9me2, and H3K27me3, which are associated with transcriptional repression (*39*). The *DOT1L* R231Q mutation only modified the methylation of histone H3K79 and did not affect the methylation status of other sites in H3 (Fig. 2D). These observations are consistent with the possibility that the *DOT1L* DOT domain mutation R231Q exerts a gain-of-function effect by enhancing its own enzyme activity in lung cancer.

The DOT1L R231Q mutant enhances H3K79me2 methylation levels and promotes malignant phenotypes

To directly determine the functional effect of the R231Q missense mutation, we used the four pairs of lung cancer cell lines to test the effects of WT DOT1L and the R231Q mutant on DOT1L substrates. The results indicated that the R231Q mutant specifically enhanced dimethylation of H3K79 (Fig. 3A and fig. S4A). Simultaneously, we also found that the R231Q mutant increased the expression of H3K79me2 in overexpressing full-length DOT1L cell model and CRISPR-introduced R231Q cell model (Fig. 3B). Then, we determined the impact of mutated DOT1L on regulating cell proliferation. Empty vector (EV), DOT1L WT, and R231Q stable cell lines were monitored using real-time cellular analysis (RTCA). We found that H460/H1299/H1975/H446-DOT1L-R231Q cells had a much greater capacity to proliferate than the WT cells (Fig. 3C and fig. S4B). Moreover, the number of colonies formed was markedly increased in cells carrying the R231Q mutation compared to the WT cells (Fig. 3D and fig. S4C). We further analyzed whether the R231Q mutation also affects cell migration and self-renewal. The results showed that cells expressing the DOT1L R231Q protein migrated in greater numbers with a higher intensity of fluorescence and formed more spheres in H460/H1299/H1975/H446-DOT1L-R231Q mutant cells compared to the WT cells (Fig. 3D and fig. S4, D and E). The ability of R231Q mutant in promoting cell proliferation and self-renewal was recapitulated in overexpressing full-length DOT1L and CRISPR-introduced R231Q cell models (Fig. 3E). Collectively, these results indicated that the capacity of DOT1L R231Q mutant cells for H3K79 dimethylation, proliferation, colony formation, migration, and self-renewal was higher than that of WT cells, which was consistent with the results of transient transfection.

Mutation of tumor-related genes can reduce the sensitivity of tumor cells to drugs and cause drug resistance. This is a major problem with the use of current antitumor drugs for cancer treatment (*9*, *40*). Therefore, we wondered whether the *DOT1L* R231Q mutation would also confer drug resistance. We selected two conventional chemotherapy drugs, cisplatin and vinorelbine, the first-line drugs for the treatment of lung cancer, and the DOT1L small-molecule inhibitor SGC0946 for in vitro and in vivo experiments (*41*). First, we treated NCI-H460-DOT1L-WT/R231Q cells with the drugs. The results of half-maximal growth inhibitory concentration (IC_{50}) analysis showed that H460 cells overexpressing DOT1L R231Q were significantly less sensitive to cisplatin, vinorelbine, and SGC0946, and the phenomenon was also observed in H1299/H1975/H446 cells overexpressing DOT1L R231Q (Fig. 3F and fig. S4F). To further validate tumor growth ability and the drug sensitivity, we established cell-derived xenograft (CDX) models in mice using three different DOT1L R231Q mutant constructed cell lines. First, we compared the tumor weight in mice receiving WT and R231Q mutant cells. We found that the tumor weight or tumor volume in the mutant groups was significantly higher than that in the WT groups (Fig. 3, G and H). This indicates that the tumor burden of the mice in the mutant group was greater, which also verified the role of DOT1L R231Q in promoting cell growth. Next, we tested the antitumor effects of cisplatin, vinorelbine, and SGC0946 on tumor weight. The tumor inhibitory effect of all three agents was significantly weaker in the mice receiving mutant cells than in the mice receiving WT cells (Fig. 3I). These results fully demonstrate that the *DOT1L* R231Q mutation induces resistance to cisplatin, vinorelbine, and SGC0946 in vitro and in vivo. Together, the data show that *DOT1L* is a lung cancer oncogene and the identified R231Q mutation could be involved in the development and progression of lung cancer, leading to malignant phenotypes.

The DOT1L R231Q mutant retains its promalignant effects when endogenous *DOT1L* is depleted

To ensure that endogenous DOT1L is not involved in the effects of R231Q mutation, we knocked down *DOT1L* in NSCLC cells and then reintroduced WT and mutant DOT1L proteins via the Tet-on system. We then detected the level of H3K79 dimethylation. In cells with knockdown of endogenous *DOT1L*, doxycycline-induced expression of the exogenous DOT1L R231Q mutant increased dimethylation of H3K79, whereas WT DOT1L caused a slight increase in H3K79me2, but less than the mutant (Fig. 4A). Moreover, we found that in the absence of inducer, the number of colonies and tumorspheres formed in *DOT1L* knockdown cells was significantly reduced. In contrast, the numbers of colonies and tumorspheres formed were significantly increased after doxycycline-induced expression of DOT1L R231Q mutant protein (Fig. 4, B and C). Moreover, the migration ability and drug resistance enhanced significantly after doxycycline-induced expression of DOT1L R231Q mutant protein (fig. S5, A and B). These findings further indicate that the R231Q mutant enhances the proliferation, self-renewal, migration ability, and drug resistance of lung cancer cells.

To continue to explore the role of the R231Q mutation in vivo, we applied the Tet-on model to animal experiments. The results showed that in the absence of doxycycline induction, the tumor growth in mice was slow, and there was no statistically significant difference in tumor growth between the WT and mutant groups (Fig. 4D). After addition of the inducer, the tumor growth rate in mice receiving the R231Q mutant cells was significantly greater than that in mice receiving WT cells (Fig. 4D). The survival time of mice in the R231Q group was significantly lower than that of mice in the WT group, and immunoblot analysis showed that the expression levels of WT DOT1L and mutant DOT1L were very similar in the two groups, while more H3K79me2 was detected in tumors from the R231Q group than in tumors from the WT group (Fig. 4, E and F). Immunohistochemistry (IHC) staining analysis of Ki67 showed that the *DOT1L* R231Q mutation induced proliferation of tumor cells (Ki67-positive cells) in mice (Fig. 4G). The TUNEL (terminal deoxynucleotidyl transferase–mediated deoxyuridine triphosphate nick end labeling) assay also demonstrated that the *DOT1L* R231Q mutation significantly reduced tumor apoptosis

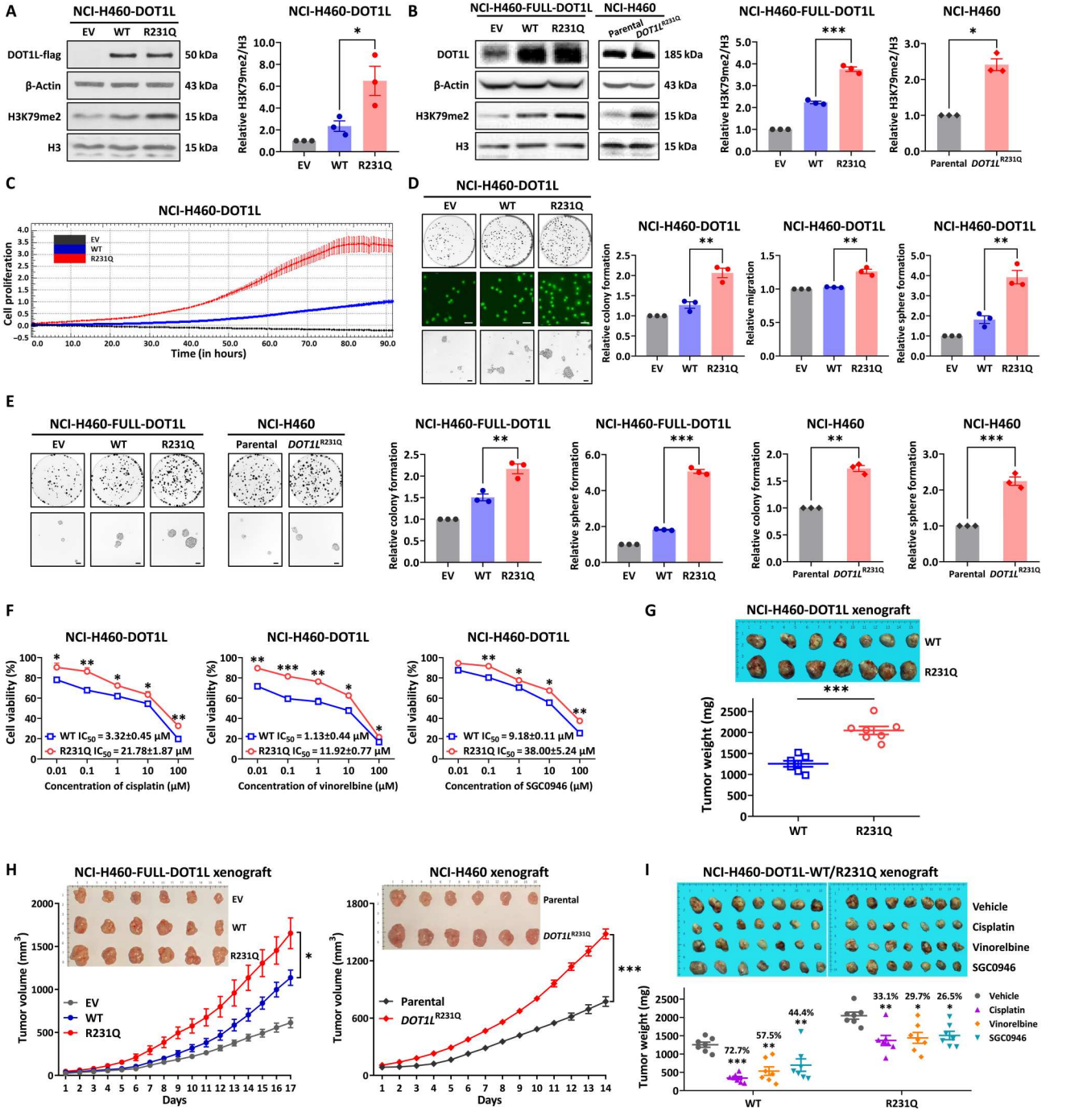

Fig. 3. DOT1L R231Q promotes lung cancer malignant phenotypes. (**A**) Western blotting analysis of tagged protein (DOT1L-flag) and H3K79me2 levels in NCI-H460-DOT1L-EV/WT/R231Q (expressing DOT1L catalytic domain). (**B**) DOT1L protein and H3K79me2 levels in NCI-H460-FULL-DOT1L-EV/WT/R231Q (expressing full-length DOT1L) or NCI-H460 *DOT1L*^{R231Q} introduced by CRISPR. (**C**) RTCA assay of NCI-H460-DOT1L-EV/WT/R231Q for 90 hours. (**D**) Crystal violet staining, Transwell assay (scale bars, 200 μm), and tumorsphere formation assay (scale bars, 1000 μm) of NCI-H460-DOT1L-EV/WT/R231Q cells. (**E**) Crystal violet staining and tumorsphere formation assay of NCI-H460-FULL-DOT1L-EV/WT/R231Q or NCI-H460 parental/*DOT1L*^{R231Q} cells. Scale bars, 1000 μm. (**F**) CCK-8 assay data showing the sensitivity of NCI-H460-DOT1L-WT/R231Q cells to cisplatin, vinorelbine, and SGC0946. Cells were treated for 72 hours (cisplatin and vinorelbine) or 6 days (SGC0946). IC_{50} values were calculated using SPSS V 21.0 software. (**G**) Tumor images and weights in the NCI-H460-DOT1L-WT/R231Q CDX model ($n = 7$ mice per group). (**H**) Tumor images and volumes in the NCI-H460-FULL-DOT1L-EV/WT/R231Q or NCI-H460 parental/*DOT1L*^{R231Q} CDX model ($n = 6$ mice per group). (**I**) CDX-bearing mice ($n = 7$ mice per group) were treated with vehicle [10% dimethyl sulfoxide (DMSO) + 40% polyethylene glycol 300 (PEG300) + 5% Tween 80 + 45% saline, five times per week], cisplatin (3 mg/kg, twice per week), vinorelbine (4 mg/kg, twice per week), or SGC0946 (20 mg/kg, five times per week) through intraperitoneal administration. The graphs show the tumor images and weights, with the tumor inhibition rate (TIR%). (TIR%) = (1 − average tumor weight after drug treatment/average tumor weight of vehicle control) × 100%. Data are shown as means ± SEM. *$P < 0.05$, **$P < 0.01$, and ***$P < 0.001$. In (A), (B), (D), and (E) to (H), P values were determined using Student's t test (independent samples t test). Data from (I) were analyzed using one-way ANOVA with Tukey's multiple comparisons test.

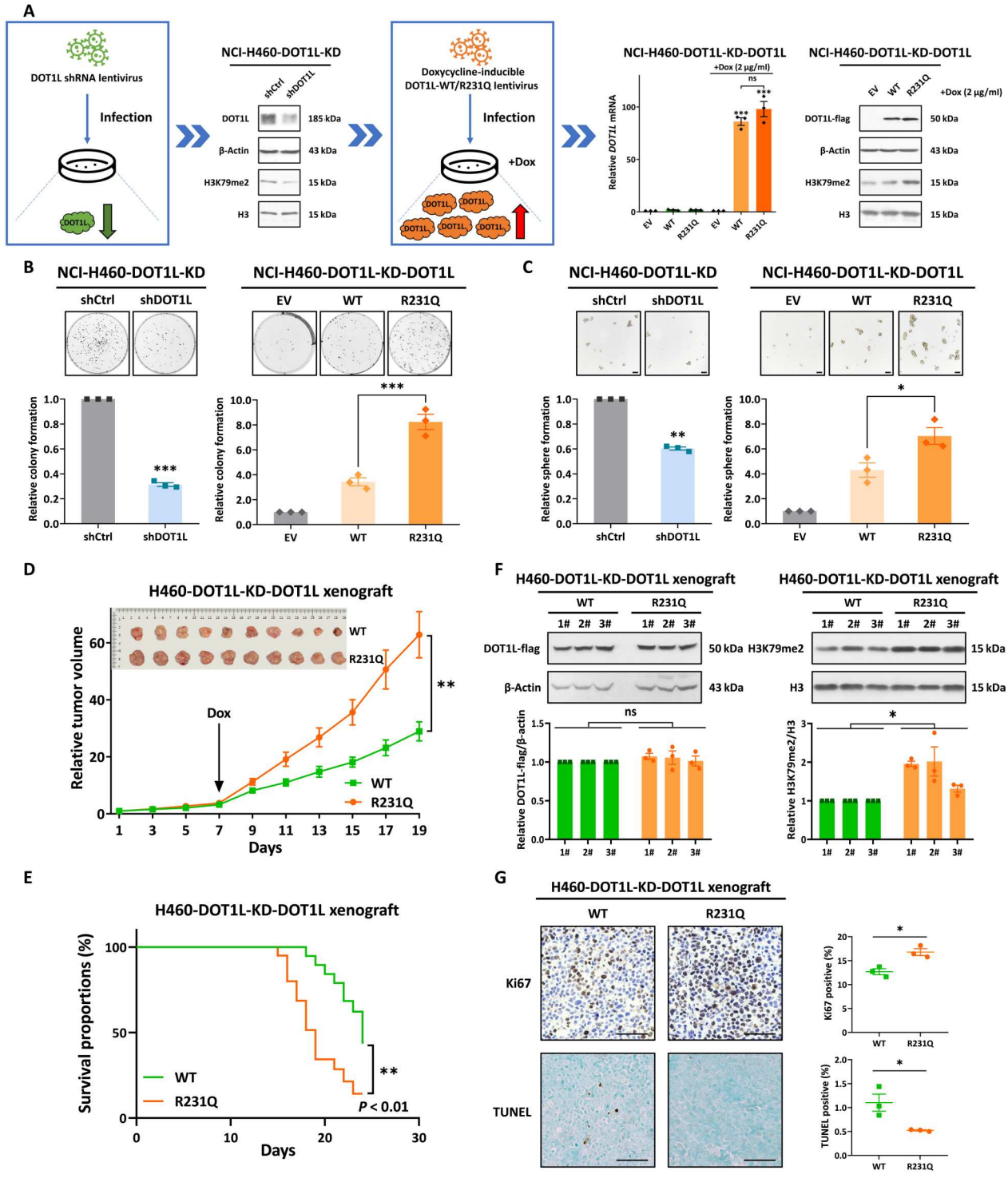

Fig. 4. In CDX mice receiving NSCLC cells with knockdown of endogenous *DOT1L*, induction of the R231Q mutant increases the malignancy of lung cancer. (**A**) *DOT1L*-depleted NSCLCs were infected with lentivirus encoding doxycycline (Dox)–inducible WT or mutant DOT1L (Tet-on system). (**B**) The cells generated in (A) were subjected to clonogenic survival assay by crystal violet staining 7 to 14 days after seeding. (**C**) The cells generated in (A) were seeded for tumorsphere formation assay and cultured for 7 to 14 days. Scale bars, 1000 μm. (**D**) Effect of doxycycline induction on the relative tumor volume in BALB/c-nu mice xenografted with NCI-H460-DOT1L-KD-DOT1L-WT/R231Q cells (n = 10 mice per group). (**E**) Survival analysis of mice in the DOT1L WT and R231Q groups (n = 20 mice per group and tumor volume > 2000 mm^3). (**F**) Western blotting analysis of DOT1L-flag and H3K79me2 expression in xenograft tumors from the CDX model in (D) (n = 3). (**G**) Ki67 staining and TUNEL staining of the CDX tumors. Scale bars, 50 μm. Data are shown as means ± SEM. *P < 0.05, **P < 0.01, and ***P < 0.001. In (A), P values were determined using one-way ANOVA with Tukey's multiple comparisons test. Data from (B) to (D), (F), and (G) were analyzed using Student's t test (independent samples t test). The log-rank (Mantel-Cox) test was used for (E), **P < 0.01.

(TUNEL-positive cells) (Fig. 4G). These results confirm that the *DOT1L* R231Q mutation increases the malignancy of lung cancer when endogenous *DOT1L* is knocked down.

DOT1L R231Q promotes lung cancer malignancy through activation of the canonical MAPK/ERK axis

To elucidate potential molecular mechanisms by which gain-of-function *DOT1L* R231Q mutation regulates proliferation and drug resistance in lung cancer, we performed gene microarray analysis in NSCLC NCI-H460 cells expressing exogenous WT or R231Q DOT1L. We observed that 546 genes were up-regulated and 184 genes were down-regulated in the mutant group compared to the WT group (Fig. 5A). Consistent with the results above, gene set enrichment analysis (GSEA) data confirmed that the differentially expressed genes were enriched in functions related to various malignant phenotypes (Fig. 5B). In addition, GSEA identified activation of previously reported oncogenic pathways associated with DOT1L, such as WNT, STAT1, and PI3K/AKT (*18*, *21*, *22*). Notably, GSEA analysis also revealed activation of some other oncogenic signaling pathways, such as the MAPK axis and the transforming growth factor–β (TGF-β) pathway (Fig. 5C). To validate these results, we treated H460-DOT1L-WT and H460-DOT1L-R231Q cells with specific signaling pathway inhibitors. The results showed that among the 12 pathway inhibitors, only RAF inhibitor (RAFi; AZ 628) and MAPK pathway inhibitors [MAPK kinase (MEK) inhibitor (MEKi) and ERK inhibitor (ERKi)] had a stronger selective anti-proliferation effect in R231Q mutant cells (Fig. 5D). Next, we examined the expression of oncogenic pathway-associated proteins in four different DOT1L R231Q mutant constructed and paired cell lines. In the R231Q mutant cell lines, we detected notable increases in important components of the MAPK signaling axis, including RAF1, phosphorylated MEK (p-MEK), and phosphorylated ERK (p-ERK) proteins (Fig. 5E and fig. S6A). However, there were no obvious changes in other pathway-related proteins in the R231Q cells compared to those in paired cells (Fig. 5E). These observations suggest that gain-of-function *DOT1L* mutation may activate canonical MAPK signaling by stimulating the expression of pathway-associated proteins.

Accumulating evidence has shown that the MAPK signaling pathway is related to the malignant phenotypes of tumors (*42*–*44*). The MAPK axis transduces extracellular signals into cells via a three-step cascade (MAPKKK→MAPKK→MAPK), thereby regulating cell biological functions including proliferation, differentiation, apoptosis, inflammation, and vascular development (*45*). We found that the RAF signaling axis is significantly enriched in cells expressing R231Q, so we used RAFi, MEKi, and ERKi (FR 180204) to investigate the proliferation, self-renewal, and drug resistance properties of DOT1L-WT and DOT1L-R231Q cells. The results showed that the number of clones and tumorspheres formed by the R231Q cells was notably reduced under treatment with RAFi, MEKi, and ERKi compared to the WT cells (Fig. 5, F and G, and fig. S6, B to D). This suggests that inhibition of the MAPK axis caused a decrease in the proliferation and self-renewal capacity of cells expressing the R231Q mutant. It is worth noting that in the H460-DOT1L-R231Q cells, MAPK inhibitor exhibited good synergistic effects with the chemotherapeutic agents, including cisplatin and vinorelbine (Fig. 5H and fig. S6E). This suggests that the resistance of H460-DOT1L-R231Q cells to cisplatin and vinorelbine was reversed under treatment with MAPK pathway inhibitors. Overall, the results further establish the MAPK axis as a mediator of DOT1L R231Q function in the malignancy of lung cancer cells.

DOT1L R231Q enriches H3K79me2 at the *RAF1* gene promoter

After demonstrating that the gain-of-function *DOT1L* R231Q mutation activates MAPK signaling, we wanted to investigate whether DOT1L R231Q regulates MAPK pathway activation by altering the enrichment of H3K79me2 on chromatin. Chromatin immunoprecipitation sequencing (ChIP-Seq) assays were performed to ascertain the genetic profile of H3K79me2 enrichment in cells. We observed that the R231Q mutation of *DOT1L* resulted in a global increase of H3K79me2 accumulation compared to DOT1L WT (Fig. 6A). The Venn diagram in Fig. 6B shows the number and overlap of genes with increased H3K79me2 levels in cells expressing DOT1L WT and R231Q. A total of 1959 genes overlapped in cells expressing WT and mutant DOT1L; however, the R231Q cells contained 3351 unique H3K79me2-enriched genes compared to 1792 unique H3K79me2-enriched genes in the WT cells. Furthermore, the H3K79me2 peak intensity was higher in cells expressing the R231Q mutant (Fig. 6B). We noticed that H3K79me2 accumulated at the *RAF1* promoter in cells expressing R231Q, and the promoter regions of *ELK3* and *KLF4*, which function downstream of MAPK, also gained H3K79me2 (Fig. 6C). We used ChIP–quantitative polymerase chain reaction (qPCR) to verify that H3K79me2 levels were higher on the *RAF1* locus in DOT1L R231Q cells than in WT cells (Fig. 6C). Next, we performed quantitative reverse transcription PCR (qRT-PCR) in cells expressing WT and mutant DOT1L to examine the mRNA expression of 29 genes involved in MAPK signaling. In DOT1L R231Q cells, 9 genes were down-regulated, and the remaining 20 genes had a trend of up-regulation. The mRNA levels of *ELK3* and *KLF4* were most strongly increased in R231Q cells (Fig. 6D). To further confirm the target genes, we measured the mRNA expression levels of the top five up-regulated genes in *DOT1L* knockdown cells and in DOT1L R231Q cells incubated with DOT1Li SGC0946. The results showed that the expression of *RAF1*, *ELK3*, and *KLF4* mRNA was reduced in *DOT1L* knockdown cells and in SGC0946-treated cells. This suggested that *DOT1L* knockdown or administration of DOT1Li reduced the level of H3K79me2, resulting in a suppressive effect on MAPK signaling. Next, we confirmed this epigenetic regulation relationship in the other cancer cell lines with low RAF1 expression. Our data showed that the expression of exogenous DOT1L R231Q protein led to increased levels of RAF1 and H3K79me2 (Fig. 6E) in HepG2 (liver cancer) and RD (rhabdomyosarcoma) cell lines. This demonstrates that R231Q activates MAPK signaling, resulting in the accumulation of H3K79 methylation in diverse cancer cells. Together, these results indicate that DOT1L R231Q favors an active chromatin state by enriching H3K79me2 at the *RAF1* promoter to increase *RAF1* expression and promote MAPK signaling.

SGC0946 is efficacious against cells expressing gain-of-function DOT1L mutants

Although some progress has been made with developing and characterizing DOT1Lis, it is currently unclear whether these inhibitors are effective against *DOT1L* gain-of-function mutations. Therefore, we tested the sensitivity of H460 cells expressing DOT1L WT and R231Q to novel synthetic and commercially available DOT1Lis. Cell Counting Kit-8 (CCK-8) assay results showed that among the

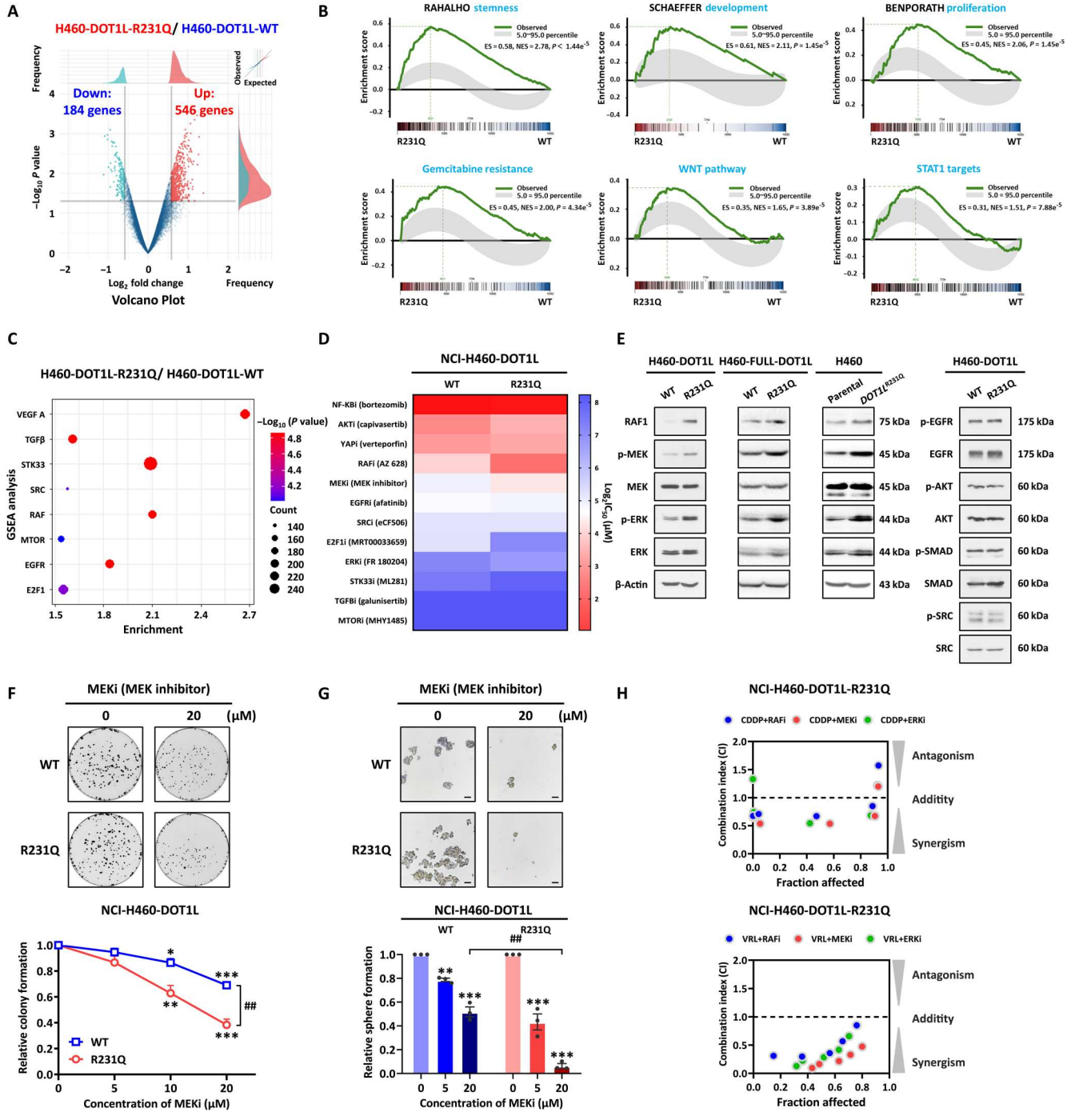

Fig. 5. DOT1L R231Q activates MAPK/ERK signaling in lung cancer. (**A**) Volcano plot showing the distribution of gene expression differences between H460 cells expressing R231Q or WT DOT1L. (**B**) GSEA analysis of the genes, which are up-regulated in H460-DOT1L-R231Q cells compared to H460-DOT1L-WT cells. GSEA identified the following gene sets: RAHALHO stemness, SCHAEFFER development, BENPORATH proliferation, gemcitabine resistance, WNT pathway, and STAT1 targets. (**C**) Bubble plot showing gene counts, *P* values, and enrichment scores of DOT1L R231Q cells versus WT cells. (**D**) Heatmap showing the effect of 12 different pathway inhibitors on DOT1L WT and R231Q cells. Cells were treated for 6 days. IC_{50} values were generated using SPSS V 21.0 software. (**E**) RAF1, p-MEK, MEK, p-ERK, and ERK expression levels were detected in NCI-H460-DOT1L-WT/R231Q (expressing DOT1L catalytic domain), NCI-H460-FULL-DOT1L-WT/R231Q (expressing full-length DOT1L), or NCI-H460 parental/*DOT1L*^{R231Q} introduced by CRISPR. In addition, p-EGFR, EGFR, p-AKT, AKT, p-SMAD2/3, SMAD2/3, p-SRC, and SRC expression levels were detected in NCI-H460-R231Q and WT cell lines. (**F** and **G**) Effect of MEKi on cell proliferation and self-renewal in NCI-H460-DOT1L-WT/R231Q cells assayed by colony formation analysis (F) and tumorsphere formation analysis (G) 7 to 14 days after seeding. Scale bars, 1000 μm. (**H**) Synergistic effect of MAPK inhibition with cisplatin or vinorelbine on NCI-H460-DOT1L-R231Q cells after 72 hours of treatment. Combination index (CI) values were calculated using the CalcuSyn program. CI < 0.90 indicates synergism, 0.90 to 1.10 indicates an additive effect, and >1.10 indicates antagonism. Data are shown as means ± SEM. **P* < 0.05, ***P* < 0.01, and ****P* < 0.001, as compared to the control group. ##*P* < 0.01, as compared to the WT group. Data from (F) and (G) were analyzed using Student's *t* test (independent samples *t* test) and one-way ANOVA with Tukey's multiple comparisons test.

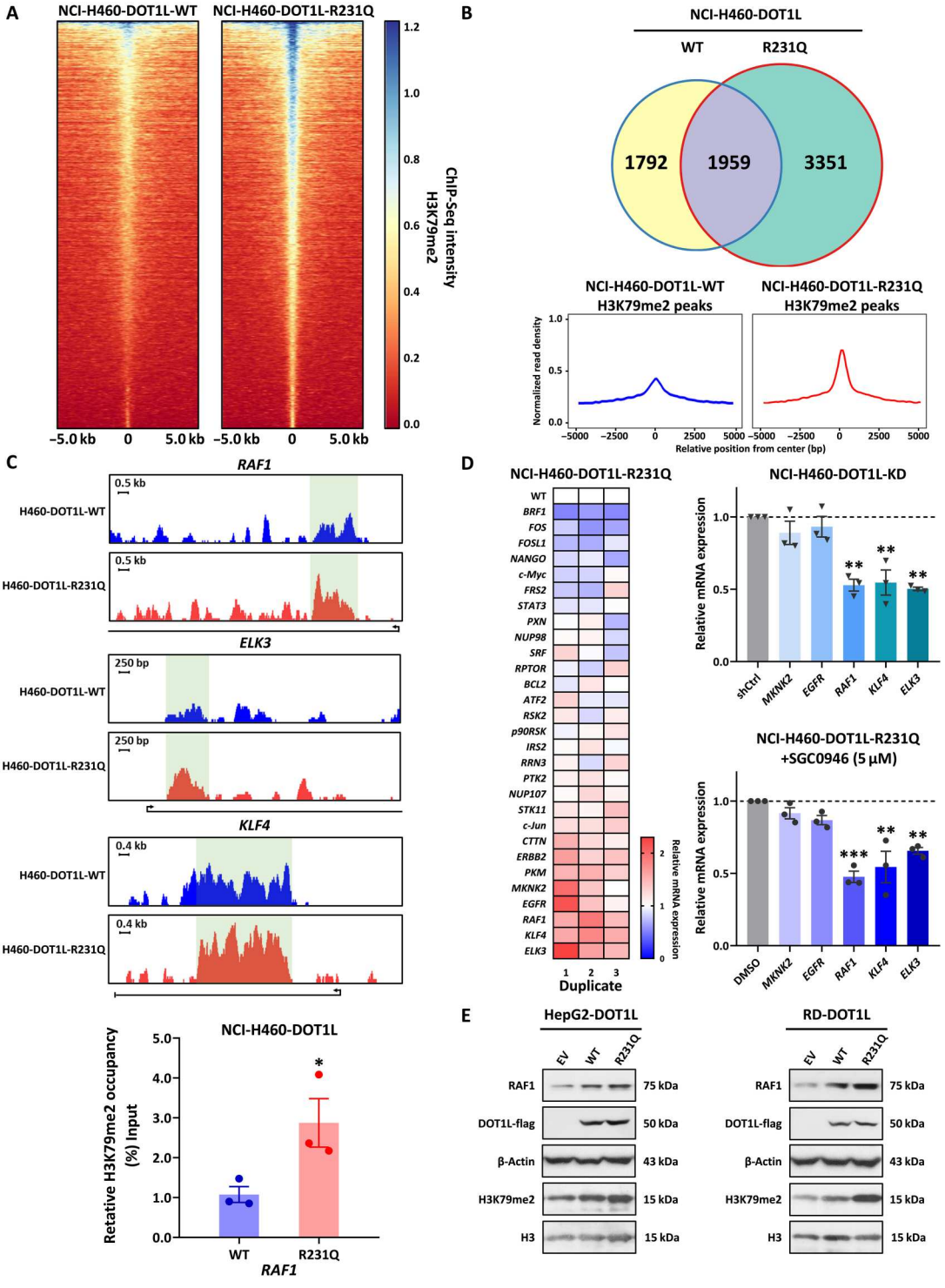

Fig. 6. DOT1L R231Q enriches H3K79me2 at the *RAF1* gene promoter. (**A**) ChIP-Seq assay results showing H3K79me2 signal intensities in cells expressing DOT1L WT and R231Q. (**B**) Venn diagram depicting the number of overlapping genes with H3K79me2 peaks in samples from cells expressing DOT1L WT or R231Q (top) and ChIP-Seq summary plot of H3K79me2 peak intensities in WT and R231Q cells (bottom). (**C**) ChIP-Seq tracks of H3K79me2 signals in the *RAF1*, *ELK3*, and *KLF4* gene loci (top) and ChIP-qPCR assay for H3K79me2 modifications at the *RAF1* locus (bottom). The green shaded areas are the H3K79me2 signals enriched in gene promoters. (**D**) Heatmap showing the relative mRNA expression levels of 29 predicted potential R231Q target genes in DOT1L WT and R231Q cells by qRT-PCR analysis (left). The expression levels of the top five up-regulated genes were then analyzed in *DOT1L* knockdown cells and R231Q cells incubated with DOT1Li SGC0946 (5 μM, 7 days). Histograms summarizing the qRT-PCR results are presented (right). (**E**) Western blotting analysis of RAF1, DOT1L-flag, and H3K79me2 expression in HepG2-DOT1L-WT/R231Q and RD-DOT1L-WT/R231Q cells. Data are shown as means ± SEM. *P < 0.05 and **P < 0.01. Data from (C) were compared using Student's t test (independent samples t test). In (D), P values were determined using one-way ANOVA with Tukey's multiple comparisons test.

numerous DOT1Lis, SGC0946 had the most potent inhibitory effect on H460-DOT1L-WT and H460-DOT1L-R231Q cells (Fig. 7A). We next simulated the binding of DOT1L and SGC0946 by molecular docking (*46*). The results showed that compared with WT DOT1L, the R231Q mutation reduced the binding energy of SGC0946 to DOT1L (Fig. 7B). This means that DOT1L R231Q has a weaker binding affinity to SGC0946 than WT, and explains why the cells expressing the R231Q mutant were more resistant to SGC0946 than the cells expressing WT DOT1L in previous experiments (Fig. 3, F and I). We subsequently compared the effects of three commercially available DOT1Lis (SGC0946, EPZ004777, and EPZ5676) on H3K79me2 levels. The results indicated that SGC0946 treatment resulted in the strongest reduction of H3K79me2 at a concentration-dependent manner (Fig. 7C and

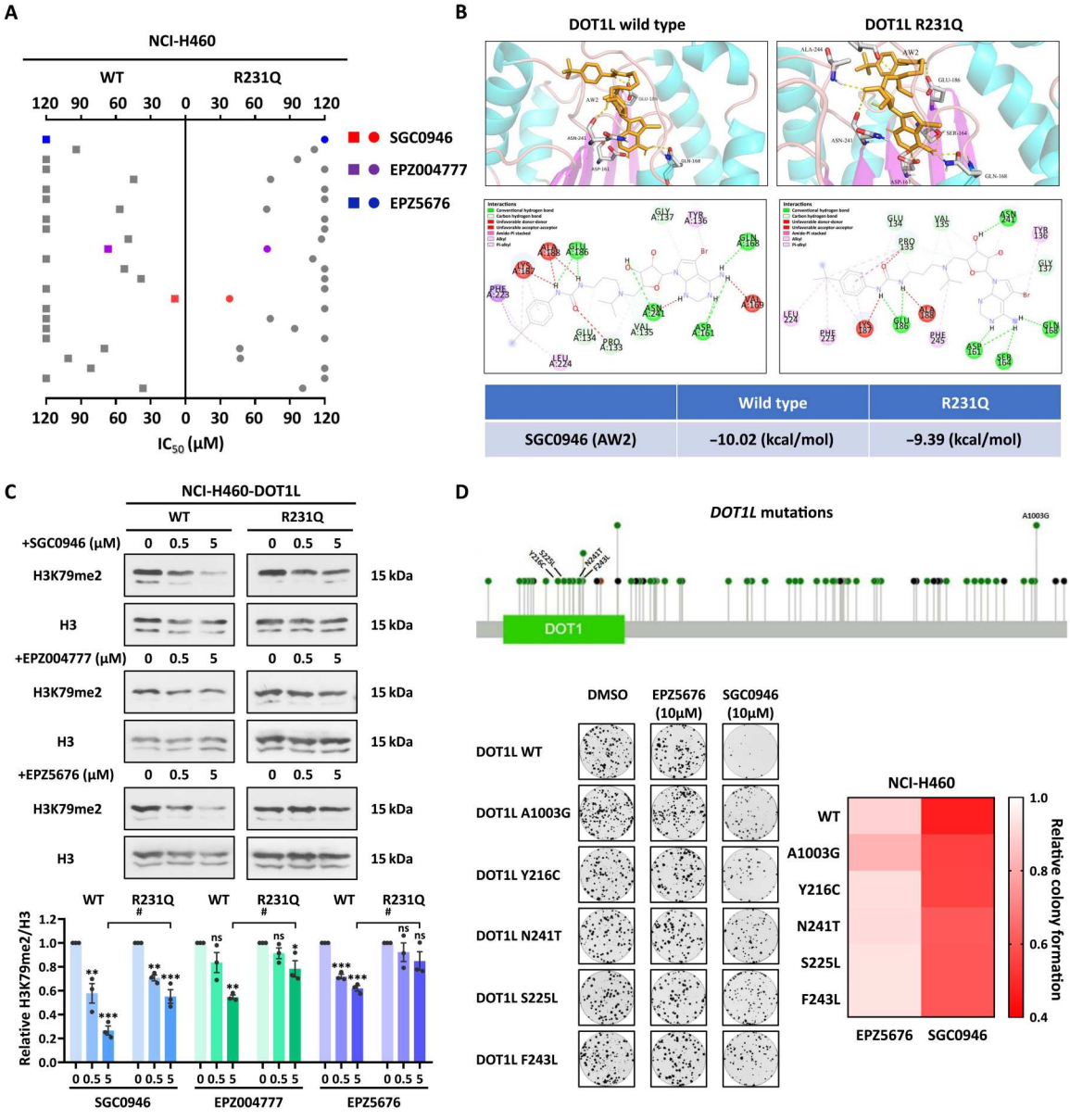

Fig. 7. SGC0946 as a candidate to inhibit gain-of-function *DOT1L* mutations. (**A**) Scatterplot summarizing the efficacy of commercially available DOT1Lis and synthetic compounds (the gray dots) using the CCK-8 assay in H460 cells expressing DOT1L WT or R231Q. Cells were treated for 6 days. The values of IC_{50} were calculated using SPSS V 21.0 software. (**B**) Binding of SGC0946 to the active site of WT and R231Q DOT1L in three-dimensional (3D) mode (top) and 2D mode (middle). The binding energy is shown at the bottom. (**C**) H3K79me2 levels in HCI-H460 cells expressing WT or R231Q DOT1L after treatment with different concentrations (0, 0.5, and 5 μM, 9 days) of DOT1Lis (SGC0946, EPZ004777, and EPZ5676). (**D**) Common gain-of-function *DOT1L* mutations in lung cancer (top) and the effects of DOT1Li SGC0946 (10 μM) or EPZ5676 (10 μM) on the colony-forming ability of cells transfected with the gain-of-function mutants Y216C, S225L, N241T, F243L, and A1003G (bottom). The number of colonies was assessed by crystal violet staining 7 to 14 days after seeding. Data are shown as means ± SEM. *$P < 0.05$, **$P < 0.01$, and ***$P < 0.001$, as compared to the control group. $^{\#}P < 0.05$, as compared to the WT group. In (C), *P* values were determined using one-way ANOVA with Tukey's multiple comparisons test and Student's *t* test (independent samples *t* test).

fig. S7A). We also analyzed the levels of H3K9me2 and H3K27me3 (fig. S7B) and found that the DOT1Lis only affected H3K79me2. In addition, SGC0946 had a stronger inhibitory effect on the proliferation of cells expressing the other DOT1L gain-of-function mutants than EPZ5676, which is already in clinical trials (Fig. 7D). This suggests that SGC0946 has great potential to inhibit DOT1L gain-of-function mutants.

Therapeutic targeting of MAPK signaling mitigates DOT1L R231Q-induced malignancy

Although SGC0946 is more effective against gain-of-function mutations than other DOT1Lis, the R231Q gain-of-function mutation still reduces the therapeutic effect of SGC0946. We provided evidence above for the molecular mechanism by which DOT1L R231Q activates MAPK signaling. Therefore, we hypothesized that MAPK axis inhibitors might be a promising approach for the

treatment of lung cancer patients harboring *DOT1L* gain-of-function mutations. Unsurprisingly, single treatment of H460-DOT1L-WT/R231Q cells with SGC0946 or binimetinib (a U.S. Food and Drug Administration–approved MEKi for melanoma) moderately inhibited cell growth. However, the combination of SGC0946 with binimetinib resulted in enhanced growth inhibition of R231Q mutant cells in vitro, and the efficiency increased with the addition of a higher dose of binimetinib (Fig. 8A). Furthermore, we found the same enhanced suppression phenomenon with the other *DOT1L* gain-of-function mutations when SGC0946 and binimetinib were used simultaneously (Fig. 8B). This suggested that the addition of MEKi increased the anti-proliferative effect of DOT1Li and reversed the resistance induced by R231Q. Next, we created four xenograft models to validate the above in vitro results. NCI-H1299-DOT1L-R231Q, NCI-H446-DOT1L-R231Q, NCI-H460-DOT1L-KD-DOT1L-R231Q, or NCI-H460 *DOT1L*^{R231Q} cells were inoculated subcutaneously into the flanks of male nude mice. The CDX-bearing mice were continuously treated with SGC0946, binimetinib, or a combination. The combination of SGC0946 and binimetinib retarded tumor growth and

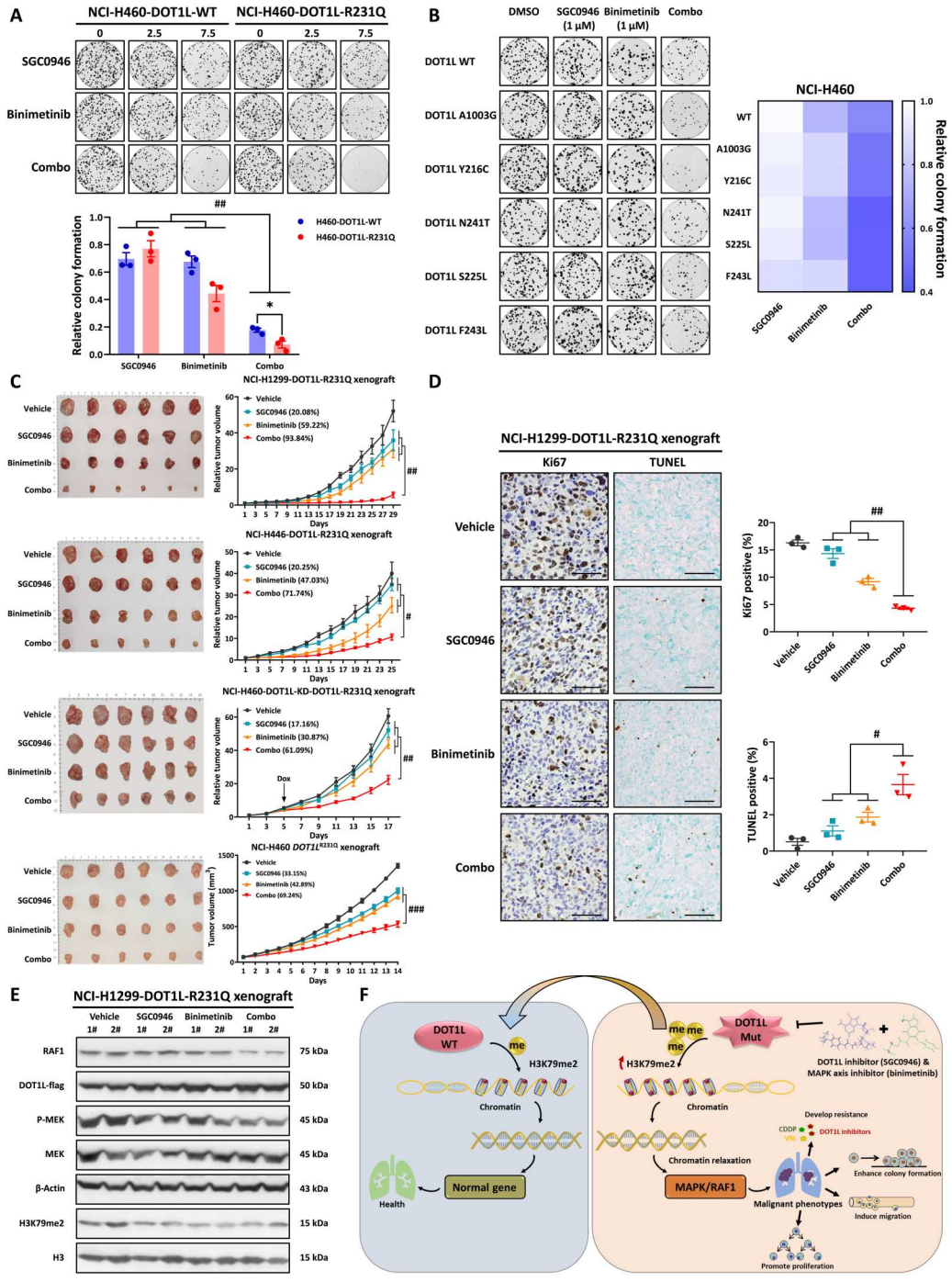

Fig. 8. Combination of SGC0946 and binimetinib inhibits proliferation of cells expressing gain-of-function DOT1L mutants in vitro and tumor growth in vivo. (**A**) Crystal violet staining of NCI-H460-DOT1L-WT/R231Q cells treated with SGC0946 (2.5 or 7.5 μM), binimetinib (2.5 or 7.5 μM), or the combination at the same concentrations for 7 to 14 days (top). Comparison of relative colony formation between groups at 7.5 μM drug concentration (bottom). (**B**) Clonogenic survival assay to evaluate the effects of DOT1Lis SGC0946 (1 μM), binimetinib (1 μM), or the combination at the same concentrations on cells transfected with constructs expressing the other DOT1L gain-of-function mutants (Y216C, S225L, N241T, F243L, and A1003G). The plates were photographed 7 to 14 days after seeding. (**C**) Tumor growth curves and images for four xenograft models (n = 6 mice per group) that were treated with vehicle (10% DMSO + 40% PEG300 + 5% Tween 80 + 45% saline, five times per week), SGC0946 (10 mg/kg, five times per week), binimetinib (15 mg/kg, five times per week), or the combination at the same doses through intraperitoneal administration and oral gavage. The graphs show the TIR%. (**D**) IHC staining for Ki67 and TUNEL staining of the NCI-H1299-DOT1L-R231Q CDX tumor tissues. Scale bars, 50 μm. (**E**) Levels of RAF1, DOT1L-flag, p-MEK, MEK, and H3K79me2 in tumors from the NCI-H1299-DOT1L-R231Q CDX mice (n = 2). (**F**) Summary diagram describing that regulation gain-of-function *DOT1L* mutations increase the malignant phenotypes of lung cancer by regulating the MAPK/ERK signaling pathway. Data are shown as means ± SEM. $^{*}P < 0.05$, as compared to the WT group. $^{\#}P < 0.05$, $^{\#\#}P < 0.01$, and $^{\#\#\#}P < 0.001$, as compared to the single treatment group. In (A), P values were determined using one-way ANOVA with Tukey's multiple comparisons test and Student's t test (independent samples t test). In (C) and (D), P values were determined using one-way ANOVA with Tukey's multiple comparisons test.

reduced the tumor burden, and the effect was highly significant compared to the single treatments (Fig. 8C). In addition, the survival time of mice in the combination group was significantly prolonged compared to the single treatments (fig. S8A). IHC staining analysis for Ki67 demonstrated that the combination therapy dramatically suppressed cell proliferation in CDX tumor tissues, and TUNEL staining demonstrated that the combination of SGC0946 and binimetinib induced apoptosis in tumor cells expressing the R231Q mutant (Fig. 8D and fig. S8, B and C). Inhibition of the activated MAPK axis by the combined SGC0946 and binimetinib therapy was further confirmed by the decreased expression levels of RAF1, p-MEK, and H3K79me2 in CDX tumor tissues (Fig. 8E and fig. S8, D and E). Together, these results confirmed that simultaneous inhibition of the MAPK axis and DOT1L is a potential therapeutic strategy for patients with *DOT1L* gain-of-function mutations.

DISCUSSION

Lung cancer, as a malignant tumor, is a serious threat to human health. Genetic mutations are the main cause of lung cancer. Gene mutations in lung cancer can be divided into two categories according to their effects. One category contains inactivating mutations of tumor suppressor genes represented by *Tp53* and *RB1*; the other category contains gain-of-function mutations represented by *KRAS* and *EGFR* oncogenic mutations (driver mutations) (*30*, *47*). The former mutations inactivate tumor suppressor genes and allow uncontrolled tumor growth, while the latter can trigger cancer progression by activating oncogenes. Current studies suggest that therapeutic strategies to restore the activity of tumor suppressor genes are difficult to achieve, while strategies to target and suppress oncogene-activating mutations are relatively feasible. This makes gain-of-function oncogenic mutations more intriguing.

Gain-of-function mutations include not only driver mutations, with high mutation rates and concentrated mutation sites, but also passenger mutations, with relatively low mutation rates and dispersed loci (*48*). Several previous studies showed that passenger mutations, similar to driver mutations, also displayed a unique functional role in the development and progression of cancer, such as being involved in the tumor plasticity and drug resistance (*49*, *50*). Similarly, recent studies reveal that mutation in genes encoding epigenetic enzymes, almost categorized as passenger mutation, can also contribute to multiple malignant phenotypes (*10*, *51*, *52*), which further demonstrates the clinical significance of passenger mutation in cancer. Here, we identified a series of gain-of-function mutations, with relatively low mutation rates, in the catalytic DOT domain of epigenetic enzyme DOT1L. Our results indicated that the gain-of-function mutations, typical example R231Q, can enhance the substrate binding ability and promote the proliferation, migration, self-renewal, and drug resistance of lung cancer cells in vitro and in vivo, which suggested their potential role in lung cancer. However, it should be noticed that the absence of patient-derived *DOT1L* mutation cell lines and the weaker phenotype for mutations other than R231Q will limit to mimic real clinical behavior and their clinical utility. Nevertheless, combined with our findings, it can still provide a new idea for understanding the role of gain-of-function mutation during oncogenesis and a potential target for lung cancer.

Molecularly targeted drug therapy has proven to be an effective strategy against tumors. DOT1L has become an important antitumor drug target due to its unique DOT catalytic domain and catalytic effect on H3K79 methylation, as well as its close relationship with tumors (*17*). In terms of activity, DOT1Lis have shown strong antitumor activity against both hematological cancers and solid tumors. Studies have found that DOT1Lis can exert antitumor effects, including inhibiting tumor cell proliferation, inducing tumor cell apoptosis, blocking tumor invasion and metastasis, inhibiting tumor stem cell self-renewal, and regulating tumor immunity (*53*, *54*). Recent studies have shown that DOT1Lis can be combined with other drugs to exert anticancer effects; for example, they can be combined with sirtuin 1 (SIRT1) activators to enhance the inhibitory effect on hematological cancers (*55*) or enhance the antitumor effect of targeted drugs (*56*). Despite this progress with DOT1Lis, it is unclear whether these inhibitors are efficacious against *DOT1L* gain-of-function mutations. We showed here that SGC0946, a commercially available inhibitor of DOT1L, had a good inhibitory effect on cells overexpressing WT DOT1L but had a relatively weak inhibitory effect on cells overexpressing the DOT1L gain-of-function mutant R231Q. Through mechanistic studies, we first demonstrated that DOT1L R231Q activated the MAPK oncogenic pathway and enriched H3K79me2 on the *RAF1* promoter. This caused changes in downstream pathway proteins, resulting in the malignant phenotype of lung cancer. This led us to hypothesize that the DOT1Li could be used in combination with a MAPK axis inhibitor.

The MAPK signaling pathway is closely related to the molecular pathogenesis of many cancers, including lung cancer, and its activation has been reported to be associated with *KRAS* and *EGFR* mutations (*45*, *57*). We found that the gain-of-function mutation R231Q, located on the DOT domain, specifically caused activation of the MAPK signaling pathway. Through the analysis of TCGA database, we found that few patients with *DOT1L* mutations had concurrent *KRAS* or *EGFR* mutations (lower than the average level in lung cancer) (fig. S9), suggesting that there may be a mutually exclusive effect between mutations. This further demonstrated that *DOT1L* mutation was the cause of MAPK pathway activation in our study. In addition, MAPK axis has been extensively reported to be relevant to the malignant phenotype, including drug resistance. Researchers have found that key molecules in MAPK axis are associated with chemotherapy, molecularly targeted drugs, and immune checkpoint inhibitor resistance (*58*, *59*). In our study, we similarly found the drug resistance induced by *DOT1L* gain-of-function mutations, which may be related to MAPK pathway activation. This implies that inhibition of MEK signaling is a promising strategy in cancer therapy.

MEKis, in combination with BRAF, KRAS, and PI3K inhibitors, have shown promising results in a variety of malignancies including mutant metastatic melanoma, *KRAS*-mutant colorectal adenocarcinoma, and *BRAF*- and *KRAS*-mutant NSCLC (*60*–*62*). Binimetinib is an oral selective inhibitor of MEK1 and MEK2 that is currently used clinically in combination with BRAF inhibitors mainly in patients with *BRAF*-mutated melanoma and colorectal cancer (*63*, *64*). The combination of binimetinib with BRAF inhibitors has shown improved efficacy (*65*). Furthermore, the efficacy of binimetinib combined with erlotinib and chemotherapeutic drugs in *KRAS* and *EGFR* mutant NSCLC patients is currently being tested in phase 2 clinical studies (*57*). This suggests that binimetinib has a strong

MAPK signaling inhibition profile and a good antitumor effect. Therefore, we chose binimetinib combined with SGC0946 to inhibit the proliferation of lung cancer cells expressing the DOT1L R231Q mutant protein in vitro and to reverse drug resistance and improve antitumor activity in vivo. Studies have shown that DOT1Li treatment can lead to feedback up-regulation of MAPK-related signaling. After the use of a DOT1Li, the proliferation of cancer cells is more dependent on the MAPK pathway (*66*). Therefore, we used the DOT1Li SGC0946 in combination with the MEKi binimetinib. This combination may also reduce the up-regulation of MAPK caused by SGC0946 alone, thus exerting an enhanced effect. The combined use of a MAPK axis inhibitor and SGC0946 is a potential approach for the treatment of lung cancer carrying a *DOT1L* gain-of-function mutation, and it is expected to become a new reference for the clinical treatment of lung cancer.

In this study, we first found that the tumor-associated mutation R231Q in the catalytic DOT domain of DOT1L is a gain-of-function mutation. The mutant protein can reshape the chromatin structure by affecting the dimethylation level of H3K79, thereby regulating the MAPK/ERK pathway. The expression of genes related to signaling pathways mediates a variety of malignant phenotype mechanisms, and the use of a DOT1Li combined with a MAPK/ERK axis inhibitor to target and regulate *DOT1L* R231Q mutations can effectively inhibit the malignancy of lung cancer (Fig. 8F). These findings will not only help to further understand the essential characteristics of lung cancer but also provide potential methods for precision treatment, thereby opening up a promising path for treating lung cancer patients.

MATERIALS AND METHODS

Study design

This study aims to discover *DOT1L* gain-of-function mutations and their molecular mechanisms in promoting malignant phenotypes in lung cancer from an epigenetic perspective. On the basis of the discovered mechanism, we can overcome lung cancer malignancy by targeting key proteins, and provide a potential therapeutic strategy for lung cancer patients harboring *DOT1L* gain-of-function mutations. We support our results based on a large number of available online databases, tissue microarray analysis, mRNA microarray, and ChIP-Seq data. For in vitro assays, we assessed the role of *DOT1L* gain-of-function mutations and epigenetic mechanisms in lung cancer using ectopic expression, lentiviral transduction, colony formation assays, RTCA, tumorsphere formation assays, migration assays, Western blotting, qRT-PCR, CCK-8 assays, molecular docking, and computer simulation. At least three independent biological replicates for each condition were used for statistical analysis. For in vivo experiments, we evaluated the functional effect of the *DOT1L* R231Q gain-of-function mutation and the antitumor effect of combination therapy in animal studies by CDX model, Western blotting, IHC staining, and TUNEL staining analysis. To minimize environmental differences and avoid experimental bias, animals were randomly assigned to control and treatment groups in a blinded manner, with no less than six animals in each experimental group to ensure statistical power. The control and treatment groups, number of biological replicates (sample size), and statistical analysis for each experiment in this article are stated in the figure legends.

Cells and cell culture

Three human NSCLC cell lines (NCI-H460, NCI-H1299, and NCI-H1975) and one human SCLC cell line (NCI-H446) were obtained from the American Type Culture Collection. NCI-H460 *DOT1L*^{R231Q} cells introduced by CRISPR-Cas9 were obtained from Cyagen Biosciences (guide RNA, GCACTATGAGGGCTGCTCGA-GGG; donor oligo, AGGCCGGGGGTCCGCGCTCACACCTGTTTTCCCTTTCAGTTGGAGAGAGGCGATTTCCTCAGCGAAGAGTGGAGGGAG**CAG**ATCGCCAACACGAGGTATGGCCAGCGTGGGGCATGCAGGGCATGTGGGGTGTGCGCTCAC) and cultured in RPMI 1640 medium (Gibco) with 10% fetal bovine serum (Gibco) and 1% penicillin-streptomycin (Gibco) at 37°C in a humidified incubator with 5% CO_2. The same culture conditions were applied to our constructs of lung cancer cell lines (NCI-H460-WT/R231Q, NCI-H1299-WT/R231Q, NCI-H1975-WT/R231Q, and NCI-H446-WT/R231Q) ectopically expressing WT or R231Q mutant DOT1L proteins (amino acids 1 to 416), the *DOT1L* knockdown NSCLC cell line (NCI-H460-DOT1L-KD), lung cancer cell lines (NCI-H460-DOT1L-KD-DOT1L-WT/R231Q) with inducible expression of DOT1L WT/R231Q (amino acids 1 to 416), and lung cancer cell lines (NCI-H460-FULL-DOT1L-WT/R231Q) ectopically expressing WT or R231Q mutant DOT1L proteins (full length).

Plasmids and compounds

The pCMV6-Entry vector, full-length *DOT1L*, *DOT1L* with point mutations (E186A, Y216C, S225L, R231Q, I232N, N241T, F243L, A1003G, and A1003S), and *DOT1L* containing different mutations at site 231 (R231A, R231M, R231W, R231K, R231N, and R231T) in the pCMV6-Entry vector were obtained from OriGene Technologies. Lentiviral expression plasmid pLVX-Puro (EV, WT, and R231Q), packaging plasmid psPAX2, and envelope plasmid pMD2G were obtained from Tsingke Biotechnology.

The series of anti-DOT1L compounds was synthesized in our laboratory as previously described. Cisplatin, vinorelbine, SGC0946, EPZ004777, EPZ5676, and binimetinib were purchased from MedChem Express (MCE).

Western blotting analysis

Cells were collected and lysed in radioimmunoprecipitation assay buffer (Cell Signaling Technology) containing 1% Protease Inhibitor Cocktail (MCE) and 1% Phosphatase Inhibitor Cocktail (MCE) or EpiQuik Total Histone Extraction Kit (EpiGentek), and protein concentration was determined using the BCA Protein Assay Kit (Thermo Fisher Scientific). Protein extracts were separated on 8 to 15% SDS–polyacrylamide gel electrophoresis (SDS-PAGE) by electrophoresis and transfer equipment (Bio-Rad) and transferred to polyvinylidene difluoride (PVDF) membranes (Millipore). The PVDF membrane was blocked and incubated with the corresponding primary and secondary antibodies, reacted with enhanced chemiluminescence (ECL) detection reagent (PerkinElmer), and exposed to x-ray films or imaging system (Azure). For the detection of proteins with the same or similar molecular weight, the primary antibody was stripped with ReBlot Plus Strong Antibody Stripping Solution (Millipore), and the corresponding primary and secondary antibodies were reincubated for chemiluminescence. Results were normalized to the internal control β-actin or histone 3. All antibody information is shown in table S1.

Transfection and lentiviral transduction

The pCMV6 recombinant plasmid was transfected into cells for 48 to 72 hours using Lipofectamine 3000 (Invitrogen) according to the manufacturer's protocol. Lentiviral expression plasmid pLVX-Puro, packaging plasmid psPAX2, and envelope plasmid pMD2G were also simultaneously transfected into 293T cells using Lipofectamine 3000 for 48 hours to produce lentivirus. Cells were seeded in six-well plates with lentivirus containing polybrene (4 μg/ml; Solarbio). Positive cells were screened with puromycin (MCE) 72 hours after infection and further characterized by Western blotting analysis.

DOT1L short hairpin RNA (shRNA) lentivirus and doxycycline-inducible DOT1L-WT/R231Q lentivirus were obtained from Obio Technology. Viruses were added to cells that had been seeded overnight in six-well plates and cultured in complete medium containing polybrene (4 μg/ml). Seventy-two hours after infection, positive cells were screened with blasticidin and puromycin (MCE), and protein expression was assessed by Western blotting.

The full-length DOT1L-WT/R231Q lentivirus was obtained from Cyagen Biosciences. Viruses were added to cells that had been seeded overnight in six-well plates and cultured in complete medium containing polybrene (4 μg/ml). Seventy-two hours after infection, positive cells were screened with puromycin (MCE), and protein expression was assessed by Western blotting.

Cell viability assay

Cells were inoculated in 96-well plates at an appropriate density and incubated with various concentrations of agents at 37°C in a 5% CO_2 incubator. CCK-8 (MCE) and multimode plate reader (Molecular Devices) were used according to the manufacturer's instructions to measure cell growth.

Colony formation assay

Cells were seeded in plates and then treated in complete medium with different concentrations of agents for 7 to 14 days. Cells were fixed with 100% methanol for 10 min, stained with 0.1% crystal violet (Sigma-Aldrich) for 30 min, and photographed (Nikon) to count the number of colonies.

Wound healing assay

Cells were seeded in 24-well plates for overnight culture. A standard 10-μl pipette tip was used to make a straight incision in the cell layer. Detached cells were removed with phosphate-buffered saline (PBS; Gibco), and the incubation was continued for 24 hours in medium containing 0.5% fetal bovine serum. Photographs of wounds were taken with an inverted microscope (Nikon) at 0 and 24 hours.

MD simulations

Using the crystal structure of DOT1L [Protein Data Bank (PDB) ID: 1NW3], two structures were prepared: DOT1L WT and DOT1L R231Q. MD simulations were run with Amber 18 software with the FF14SB force field for protein and ions, and the TIP3P model for water. The protein system water molecules were appended to a cube with periodic boundary conditions, while counterions (Na^+) were added to maintain the electrical neutrality of the overall system. The particle mesh Ewald algorithm was used for energy minimization, and MD was used to calculate the long-range electrostatic interactions with a cutoff value of 10 Å in the whole simulation process. The SHAKE algorithm was applied to constrain all the covalent bonds with hydrogens, and Langevin dynamics with a collision frequency γ of 1.0 was used to control the change of temperature during MD simulation. The energy of the system is minimized first to remove the bad contact caused by the addition of water. In the process of energy minimization, first, the solute was confined [the protein was immobilized, the binding force constant is 2 kcal/(mol $Å^{-2}$)], the system was optimized with 5000 steps of steepest descent method, and then a maximum of 5000 steps of conjugate gradient method optimization was performed. Next, without limiting the force, the entire system was let go and the same energy minimization was performed. Then, the system was heated from 0 to 300 K within 100 ps and then dynamic equilibrium was performed at room temperature (300 K) and atmospheric pressure (1 atm) for 100 ns.

Molecular docking

Docking calculations were performed with the AutoDock program 4.2. The small drug molecule SGC0946 (AW2) was docked with the crystal structure of DOT1L protein (PDB:1NW3) and the mutant R231Q. The grid box was defined as a cubic binding pocket with 50 points for every side in the grid spacing of 0.375 Å. Two hundred binding poses were calculated through the genetic algorithm with 2.5×10^7 maximum number of evaluations and 150 population size. The default parameters were used for other options.

Real-time cell analysis

Cells were seeded in E-Plates after the baseline had been measured and cultured in complete medium. Cell proliferation was detected using an xCELLigence analyzer system (ACEA Biosciences) according to the manufacturer's instructions.

Transwell migration assay

Using Transwell Permeable Supports (Corning) according to the manufacturer's instructions, single-cell suspensions that had been starved overnight were seeded in the upper chamber containing serum-free medium. Complete medium was added to the lower chamber. After incubation for 48 hours, cells were fluorescently labeled with Calcein AM (Sigma-Aldrich), photographed (Nikon), and counted.

Tumorsphere formation assay

Cells from different groups were digested into suspensions, and single cells were counted and seeded into low-attachment surface six-well plates (Corning) containing 2 ml per well of serum-free stem cell medium (Gibco). The cultures were supplemented with 0.2 ml of stem cell medium every 3 days. The number of tumorspheres containing more than 50 cells was counted and photographed on days 7 to 14 to examine the self-renewal ability of tumor cells.

In vivo xenograft model

In CDX studies, 1×10^6 to 2×10^6 cells suspended in PBS (Gibco) containing Matrigel (BD Biosciences) were inoculated subcutaneously into the right flank of 6- to 8-week-old male BALB/c-nu mice, and visible tumors were measured with digital calipers. When the average tumor volume reached 50 to 80 mm^3, the mice were randomly divided into the control group and different treatment groups. The tumor size and body weight were measured every day or every 2 days, and the tumor volume was calculated using the formula volume = 0.5 × length × $width^2$. At the end of the

experiment, the mice were sacrificed, and the tumors were weighed and stored at 80°C or fixed in formalin for subsequent determination of tumor tissue protein expression or IHC. These experiments were performed in strict accordance with the recommendations in the *Guide for the Care and Use of Laboratory Animals* of the National Institutes of Health, and the corresponding protocols were approved by the Animal Experimentation Ethics Committee of Shenyang Pharmaceutical University.

RNA isolation and qRT-PCR

Total RNA was extracted from cells using TRIzol reagent (Thermo Fisher Scientific) according to the manufacturer's instructions, and the RNA concentration was determined using NanoDrop (Thermo Fisher Scientific) and reverse-transcribed into complementary DNA (cDNA) by the Revert Aid First Strand cDNA Synthesis Kit (Thermo Fisher Scientific). qRT-PCR was performed using the SYBR Green Supermix Kit (Thermo Fisher Scientific) in Bio-Rad PCR equipment. Glyceraldehyde-3-phosphate dehydrogenase (GAPDH) served as the internal control, and gene expression levels were determined using the $2^{-\Delta\Delta Ct}$ method. All primer sequences are shown in table S2.

IHC and TUNEL assay

Patient tissue microarrays were obtained from Outdo Biotech Company. A total of 98 patients participated in this study; they had NSCLC (stage I and stage III) and received treatment between September 2004 and April 2009. Clinical specimens used in this study were approved by the Committee for Ethical Review of Research Involving Human Subjects at Shanghai Biochip National Engineering Research Center (Outdo Biotech Company, ethical number: YB M-05-02). Written informed consent was obtained from all patients. Specimens were scored according to the intensity of staining and the percentage of positive cells. Staining intensity was graded as 0 (no color), 1 (light color), 2 (light brown), or 3 (brown). The percentage of positive cells was graded as 0 (<5%), 1 (5 to 25%), 2 (26 to 50%), 3 (51 to 75%), or 4 (>75%). The above two scores were summed, and the average score was calculated: Higher than the average score was designated as high expression, and lower than the average score was designated as low expression. Animal tumor tissues were derived from xenograft models. Animal tumor tissue was formalin-fixed and dehydrated. After paraffin embedding, tumors were cut into 5-μm-thick sections with a microtome (Thermo Fisher Scientific) for antigen retrieval. Following blocking of endogenous peroxidase activity using the Immunohistochemical Kit (ZSGB-BIO) according to the manufacturer's protocol, tissue sections were blocked, coincubated with appropriate primary and secondary antibodies, and reacted with Diaminobenzidine (DAB) reagents. Photographs were taken for observation (Leica), and the positive cells were statistically analyzed.

Apoptosis in tumor sections of xenograft models was detected using the TUNEL Assay Kit-HRP-DAB (Abcam) according to the manufacturer's protocol. Positive nuclei were stained brown and photographed (Leica), and the percentage of positive cells was calculated.

mRNA microarray analysis

Total RNA was extracted from NCI-H460-DOT1L-WT/R231Q cells using TRIzol reagent (Thermo Fisher Scientific). Data from mRNA microarrays were obtained from Baygene Biotechnologies and analyzed to identify differentially expressed genes between cells expressing WT and R231Q mutant DOT1L.

Chromatin immunoprecipitation

According to the manufacturer's instructions, the DNA bound to H3K79me2 was obtained using the ChIP Kit (Cell Signaling Technology). Amogene Biotechnology was commissioned to perform ChIP-Seq analysis of H3K79me2-enriched genes in cells with WT and R231Q mutant DOT1L. On the basis of the ChIP-Seq results, Tsingke Biotechnology was commissioned to design *RAF1* promoter primers for qPCR analysis of DNA isolated from the ChIP assay.

Statistical analysis

All in vitro experiments were repeated at least three times, and data were analyzed using GraphPad Prism version 8.0 and presented as means ± SEM. All animal experiments were performed once, and each tumor graft was an independent sample for in vivo experiments. Statistical analysis was performed using SPSS V 21.0 software. Data were compared using Student's *t* test (independent samples *t* test) or one-way analysis of variance (ANOVA), followed by Tukey's multiple comparisons test. $^{*}P < 0.05$, $^{**}P < 0.01$, and $^{***}P < 0.001$.

Supplementary Materials

This PDF file includes:
Figs. S1 to S9
Tables S1 and S2
Legend for data file S1

Other Supplementary Material for this manuscript includes the following:
Data file S1

REFERENCES AND NOTES

1. R. L. Siegel, K. D. Miller, H. E. Fuchs, A. Jemal, Cancer statistics, 2022. *CA Cancer J. Clin.* **72**, 7–33 (2022).
2. A. A. Thai, B. J. Solomon, L. V. Sequist, J. F. Gainor, R. S. Heist, Lung cancer. *Lancet* **398**, 535–554 (2021).
3. W. Wang, M. Zhao, L. Cui, Y. Ren, J. Zhang, J. Chen, L. Jia, J. Zhang, J. Yang, G. Chen, C. R. Ashby Jr., C. Wu, Z. S. Chen, L. Wang, Characterization of a novel HDAC/RXR/HtrA1 signaling axis as a novel target to overcome cisplatin resistance in human non-small cell lung cancer. *Mol. Cancer* **19**, 134 (2020).
4. M. G. Oser, M. J. Niederst, L. V. Sequist, J. A. Engelman, Transformation from non-small-cell lung cancer to small-cell lung cancer: Molecular drivers and cells of origin. *Lancet Oncol.* **16**, e165–e172 (2015).
5. W. H. Hsu, J. C. Yang, T. S. Mok, H. H. Loong, Overview of current systemic management of EGFR-mutant NSCLC. *Ann. Oncol.* **29**, i3–i9 (2018).
6. J. Yun, S. H. Lee, S. Y. Kim, S. Y. Jeong, J. H. Kim, K. H. Pyo, C. W. Park, S. G. Heo, M. R. Yun, S. Lim, S. M. Lim, M. H. Hong, H. R. Kim, M. Thayu, J. C. Curtin, R. E. Knoblauch, M. V. Lorenzi, A. Roshak, B. C. Cho, Antitumor activity of amivantamab (JNJ-61186372), an EGFR-MET bispecific antibody, in diverse models of EGFR exon 20 insertion-driven NSCLC. *Cancer Discov.* **10**, 1194–1209 (2020).
7. Y. Jia, C. H. Yun, E. Park, D. Ercan, M. Manuia, J. Juarez, C. Xu, K. Rhee, T. Chen, H. Zhang, S. Palakurthi, J. Jang, G. Lelais, M. DiDonato, B. Bursulaya, P. Y. Michellys, R. Epple, T. H. Marsilje, M. McNeill, W. Lu, J. Harris, S. Bender, K. K. Wong, P. A. Janne, M. J. Eck, Overcoming EGFR(T790M) and EGFR(C797S) resistance with mutant-selective allosteric inhibitors. *Nature* **534**, 129–132 (2016).
8. Z. Piotrowska, M. J. Niederst, C. A. Karlovich, H. A. Wakelee, J. W. Neal, M. Mino-Kenudson, L. Fulton, A. N. Hata, E. L. Lockerman, A. Kalsy, S. Digumarthy, A. Muzikansky, M. Raponi, A. R. Garcia, H. E. Mulvey, M. K. Parks, R. H. DiCecca, D. Dias-Santagata, A. J. Iafrate, A. T. Shaw, A. R. Allen, J. A. Engelman, L. V. Sequist, Heterogeneity underlies the emergence of

EGFRT790 wild-type clones following treatment of T790M-positive cancers with a third-generation EGFR inhibitor. *Cancer Discov.* **5**, 713–722 (2015).
9. H. Zhang, A. Schaefer, Y. Wang, R. G. Hodge, D. R. Blake, J. N. Diehl, A. G. Papageorge, M. D. Stachler, J. Liao, J. Zhou, Z. Wu, F. G. Akarca, L. K. de Klerk, S. Derks, M. Pierobon, K. A. Hoadley, T. C. Wang, G. Church, K. K. Wong, E. F. Petricoin, A. D. Cox, D. R. Lowy, C. J. Der, A. J. Bass, Gain-of-function RHOA mutations promote focal adhesion kinase activation and dependency in diffuse gastric cancer. *Cancer Discov.* **10**, 288–305 (2020).
10. S. Kato, Q. Y. Weng, M. L. Insco, K. Y. Chen, S. Muralidhar, J. Pozniak, J. M. S. Diaz, Y. Drier, N. Nguyen, J. A. Lo, E. van Rooijen, L. V. Kemeny, Y. Zhan, Y. Feng, W. Silkworth, C. T. Powell, B. B. Liau, Y. Xiong, J. Jin, J. Newton-Bishop, L. I. Zon, B. E. Bernstein, D. E. Fisher, Gain-of-function genetic alterations of G9a drive oncogenesis. *Cancer Discov.* **10**, 980–997 (2020).
11. Y. Sun, X. Bao, Y. Ren, L. Jia, S. Zou, J. Han, M. Zhao, M. Han, H. Li, Q. Hua, Y. Fang, J. Yang, C. Wu, G. Chen, L. Wang, Targeting HDAC/OAZ1 axis with a novel inhibitor effectively reverses cisplatin resistance in non-small cell lung cancer. *Cell Death Dis.* **10**, 400 (2019).
12. L. Wang, X. Dong, Y. Ren, J. Luo, P. Liu, D. Su, X. Yang, Targeting EHMT2 reverses EGFR-TKI resistance in NSCLC by epigenetically regulating the PTEN/AKT signaling pathway. *Cell Death Dis.* **9**, 129 (2018).
13. B. Zhu, S. Chen, H. Wang, C. Yin, C. Han, C. Peng, Z. Liu, L. Wan, X. Zhang, J. Zhang, C. G. Lian, P. Ma, Z.-X. Xu, S. Prince, T. Wang, X. Gao, Y. Shi, D. Liu, M. Liu, W. Wei, Z. Wei, J. Pan, Y. Wang, Z. Xuan, J. Hess, N. K. Hayward, C. R. Goding, X. Chen, J. Zhou, R. Cui, The protective role of DOT1L in UV-induced melanomagenesis. *Nat. Commun.* **9**, 259 (2018).
14. L. Godfrey, N. T. Crump, R. Thorne, I. J. Lau, E. Repapi, D. Dimou, A. L. Smith, J. R. Harman, J. M. Telenius, A. M. Oudelaar, D. J. Downes, P. Vyas, J. R. Hughes, T. A. Milne, DOT1L inhibition reveals a distinct subset of enhancers dependent on H3K79 methylation. *Nat. Commun.* **10**, 2803 (2019).
15. G. Nassa, A. Salvati, R. Tarallo, V. Gigantino, E. Alexandrova, D. Memoli, A. Sellitto, F. Rizzo, D. Malanga, T. Mirante, E. Morelli, M. Nees, M. Åkerfelt, S. Kangaspeska, T. A. Nyman, L. Milanesi, G. Giurato, A. Weisz, Inhibition of histone methyltransferase DOT1L silences ERα gene and blocks proliferation of antiestrogen-resistant breast cancer cells. *Sci. Adv.* **5**, eaav5590 (2019).
16. L. Yang, Q. Lei, L. Li, J. Yang, Z. Dong, H. Cui, Silencing or inhibition of H3K79 methyltransferase DOT1L induces cell cycle arrest by epigenetically modulating c-Myc expression in colorectal cancer. *Clin. Epigenetics* **11**, 199 (2019).
17. S. R. Daigle, E. J. Olhava, C. A. Therkelsen, A. Basavapathruni, L. Jin, P. A. Boriack-Sjodin, C. J. Allain, C. R. Klaus, A. Raimondi, M. P. Scott, N. J. Waters, R. Chesworth, M. P. Moyer, R. A. Copeland, V. M. Richon, R. M. Pollock, Potent inhibition of DOT1L as treatment of MLL-fusion leukemia. *Blood* **122**, 1017–1025 (2013).
18. Y. Liu, J. Z. Guo, Y. Liu, K. Wang, W. Ding, H. Wang, X. Liu, S. Zhou, X. C. Lu, H. B. Yang, C. Xu, W. Gao, L. Zhou, Y. P. Wang, W. Hu, Y. Wei, C. Huang, Q. Y. Lei, Nuclear lactate dehydrogenase A senses ROS to produce α-hydroxybutyrate for HPV-induced cervical tumor growth. *Nat. Commun.* **9**, 4429 (2018).
19. A. Salvati, V. Gigantino, G. Nassa, G. Giurato, E. Alexandrova, F. Rizzo, R. Tarallo, A. Weisz, The histone methyltransferase DOT1L is a functional component of estrogen receptor alpha signaling in ovarian cancer cells. *Cancers (Basel)* **11**, 1720 (2019).
20. D. Liu, X. X. Zhang, M. C. Li, C. H. Cao, D. Y. Wan, B. X. Xi, J. H. Tan, J. Wang, Z. Y. Yang, X. X. Feng, F. Ye, G. Chen, P. Wu, L. Xi, H. Wang, J. F. Zhou, Z. H. Feng, D. Ma, Q. L. Gao, C/EBPβ enhances platinum resistance of ovarian cancer cells by reprogramming H3K79 methylation. *Nat. Commun.* **9**, 1739 (2018).
21. S. Shah, M. A. Henriksen, A novel disrupter of telomere silencing 1-like (DOT1L) interaction is required for signal transducer and activator of transcription 1 (STAT1)-activated gene expression. *J. Biol. Chem.* **286**, 41195–41204 (2011).
22. C. Yang, Z. Chen, H. Yu, X. Liu, Inhibition of disruptor of telomeric silencing 1-like alleviated renal ischemia and reperfusion injury-induced fibrosis by blocking PI3K/AKT-mediated oxidative stress. *Drug Des. Devel. Ther.* **13**, 4375–4387 (2019).
23. W. Kim, R. Kim, G. Park, J. W. Park, J. E. Kim, Deficiency of H3K79 histone methyltransferase Dot1-like protein (DOT1L) inhibits cell proliferation. *J. Biol. Chem.* **287**, 5588–5599 (2012).
24. M. Serresi, S. Kertalli, L. Li, M. Schmitt, Y. Dramaretska, J. Wierikx, D. Hulsman, G. Gargiulo, Functional antagonism of chromatin modulators regulates epithelial-mesenchymal transition. *Sci. Adv.* **7**, eabd7974 (2021).
25. J. Xu, Y. Wang, Y. Dai, W. Zhang, W. Zhang, S. Xiong, Z. Gu, K. Wang, R. Zeng, Z. Chen, S. Chen, DNMT3A Arg^{882} mutation drives chronic myelomonocytic leukemia through disturbing gene expression/DNA methylation in hematopoietic cells. *Proc. Natl. Acad. Sci. U.S.A.* **111**, 2620–2625 (2014).
26. G. P. Souroullas, W. R. Jeck, J. S. Parker, J. M. Simon, J. Y. Liu, J. Paulk, J. Xiong, K. S. Clark, Y. Fedoriw, J. Qi, C. E. Burd, J. E. Bradner, N. E. Sharpless, An oncogenic Ezh2 mutation induces tumors through global redistribution of histone 3 lysine 27 trimethylation. *Nat. Med.* **22**, 632–640 (2016).
27. J. D. Campbell, A. Alexandrov, J. Kim, J. Wala, A. H. Berger, C. S. Pedamallu, S. A. Shukla, G. Guo, A. N. Brooks, B. A. Murray, M. Imielinski, X. Hu, S. Ling, R. Akbani, M. Rosenberg, C. Cibulskis, A. Ramachandran, E. A. Collisson, D. J. Kwiatkowski, M. S. Lawrence, J. N. Weinstein, R. G. Verhaak, C. J. Wu, P. S. Hammerman, A. D. Cherniack, G. Getz; N. Cancer Genome Atlas Research, M. N. Artyomov, R. Schreiber, R. Govindan, M. Meyerson, Distinct patterns of somatic genome alterations in lung adenocarcinomas and squamous cell carcinomas. *Nat. Genet.* **48**, 607–616 (2016).
28. E. Cerami, J. Gao, U. Dogrusoz, B. E. Gross, S. O. Sumer, B. A. Aksoy, A. Jacobsen, C. J. Byrne, M. L. Heuer, E. Larsson, Y. Antipin, B. Reva, A. P. Goldberg, C. Sander, N. Schultz, The cBio cancer genomics portal: An open platform for exploring multidimensional cancer genomics data. *Cancer Discov.* **2**, 401–404 (2012).
29. M. Mohan, H. M. Herz, Y. H. Takahashi, C. Lin, K. C. Lai, Y. Zhang, M. P. Washburn, L. Florens, A. Shilatifard, Linking H3K79 trimethylation to Wnt signaling through a novel Dot1-containing complex (DotCom). *Genes Dev.* **24**, 574–589 (2010).
30. F. Skoulidis, J. V. Heymach, Co-occurring genomic alterations in non-small-cell lung cancer biology and therapy. *Nat. Rev. Cancer* **19**, 495–509 (2019).
31. K. C. Arbour, G. J. Riely, Systemic therapy for locally advanced and metastatic non-small cell lung cancer: A review. *JAMA* **322**, 764–774 (2019).
32. J. Min, Q. Feng, Z. Li, Y. Zhang, R.-M. Xu, Structure of the catalytic domain of human DOT1L, a non-SET domain nucleosomal histone methyltransferase. *Cell* **112**, 711–723 (2003).
33. D. Seeliger, B. L. de Groot, Ligand docking and binding site analysis with PyMOL and Autodock/Vina. *J. Comput. Aided Mol. Des.* **24**, 417–422 (2010).
34. W. Tian, C. Chen, X. Lei, J. Zhao, J. Liang, CASTp 3.0: Computed atlas of surface topography of proteins: Computed atlas of surface topography of proteins. *Nucleic Acids Res.* **46**, W363–W367 (2018).
35. T. S. Lee, D. S. Cerutti, D. Mermelstein, C. Lin, S. LeGrand, T. J. Giese, A. Roitberg, D. A. Case, R. C. Walker, D. M. York, GPU-accelerated molecular dynamics and free energy methods in amber18: Performance enhancements and new features. *J. Chem. Inf. Model.* **58**, 2043–2050 (2018).
36. K. M. Bernt, N. Zhu, A. U. Sinha, S. Vempati, J. Faber, A. V. Krivtsov, Z. Feng, N. Punt, A. Daigle, L. Bullinger, R. M. Pollock, V. M. Richon, A. L. Kung, S. A. Armstrong, MLL-rearranged leukemia is dependent on aberrant H3K79 methylation by DOT1L. *Cancer Cell* **20**, 66–78 (2011).
37. H. Alam, M. Tang, M. Maitituoheti, S. S. Dhar, M. Kumar, C. Y. Han, C. R. Ambati, S. B. Amin, B. Gu, T. Y. Chen, Y. H. Lin, J. Chen, F. L. Muller, N. Putluri, E. R. Flores, F. J. DeMayo, L. Baseler, K. Rai, M. G. Lee, KMT2D deficiency impairs super-enhancers to confer a glycolytic vulnerability in lung cancer. *Cancer Cell* **37**, 599–617.e7 (2020).
38. H. Vlaming, C. M. McLean, T. Korthout, M. F. Alemdehy, S. Hendriks, C. Lancini, S. Palit, S. Klarenbeek, E. M. Kwesi-Maliepaard, T. M. Molenaar, L. Hoekman, T. T. Schmidlin, A. M. Altelaar, T. van Welsem, J. H. Dannenberg, H. Jacobs, F. van Leeuwen, Conserved crosstalk between histone deacetylation and H3K79 methylation generates DOT1L-dose dependency in HDAC1-deficient thymic lymphoma. *EMBO J.* **38**, e101564 (2019).
39. A. T. Nguyen, Y. Zhang, The diverse functions of Dot1 and H3K79 methylation. *Genes Dev.* **25**, 1345–1358 (2011).
40. Y. Gao, A. Maria, N. Na, A. da Cruz Paula, A. N. Gorelick, J. F. Hechtman, J. Carson, R. A. Lefkowitz, B. Weigelt, B. S. Taylor, H. Zhao, J. S. Reis-Filho, E. de Stanchina, N. Rosen, Z. Yao, R. Yaeger, V211D mutation in MEK1 causes resistance to MEK inhibitors in colon cancer. *Cancer Discov.* **9**, 1182–1191 (2019).
41. S. Ghosh, Cisplatin: The first metal based anticancer drug. *Bioorg. Chem.* **88**, 102925 (2019).
42. T. Jiang, Y. Xia, J. Lv, B. Li, Y. Li, S. Wang, Z. Xuan, L. Xie, S. Qiu, Z. He, L. Wang, Z. Xu, A novel protein encoded by circMAPK1 inhibits progression of gastric cancer by suppressing activation of MAPK signaling. *Mol. Cancer* **20**, 66 (2021).
43. K. Deng, L. Liu, X. Tan, Z. Zhang, J. Li, Y. Ou, X. Wang, S. Yang, R. Xiang, P. Sun, WIP1 promotes cancer stem cell properties by inhibiting p38 MAPK in NSCLC. *Signal Transduct. Target. Ther.* **5**, 36 (2020).
44. L. G. Ahronian, E. M. Sennott, E. M. Van Allen, N. Wagle, E. L. Kwak, J. E. Faris, J. T. Godfrey, K. Nishimura, K. D. Lynch, C. H. Mermel, E. L. Lockerman, A. Kalsy, J. M. Gurski Jr., S. Bahl, K. Anderka, L. M. Green, N. J. Lennon, T. G. Huynh, M. Mino-Kenudson, G. Getz, D. Dias-Santagata, A. J. Iafrate, J. A. Engelman, L. A. Garraway, R. B. Corcoran, Clinical acquired resistance to RAF inhibitor combinations in BRAF-mutant colorectal cancer through MAPK pathway alterations. *Cancer Discov.* **5**, 358–367 (2015).
45. M. Drosten, M. Barbacid, Targeting the MAPK pathway in KRAS-driven tumors. *Cancer Cell* **37**, 543–550 (2020).
46. G. M. Morris, R. Huey, W. Lindstrom, M. F. Sanner, R. K. Belew, D. S. Goodsell, A. J. Olson, AutoDock4 and autoDockTools4: Automated docking with selective receptor flexibility. *J. Comput. Chem.* **30**, 2785–2791 (2009).
47. Q. S. Chu, Targeting non-small cell lung cancer: Driver mutation beyond epidermal growth factor mutation and anaplastic lymphoma kinase fusion. *Ther. Adv. Med. Oncol.* **12**, 1758835919895756 (2020).

48. F. Dietlein, A. B. Wang, C. Fagre, A. Tang, N. J. M. Besselink, E. Cuppen, C. Li, S. R. Sunyaev, J. T. Neal, E. M. Van Allen, Genome-wide analysis of somatic noncoding mutation patterns in cancer. *Science* **376**, eabg5601 (2022).
49. E. J. Adams, W. R. Karthaus, E. Hoover, D. Liu, A. Gruet, Z. Zhang, H. Cho, R. DiLoreto, S. Chhangawala, Y. Liu, P. A. Watson, E. Davicioni, A. Sboner, C. E. Barbieri, R. Bose, C. S. Leslie, C. L. Sawyers, FOXA1 mutations alter pioneering activity, differentiation and prostate cancer phenotypes. *Nature* **571**, 408–412 (2019).
50. E. Elez, J. Ros, J. Fernandez, G. Villacampa, A. B. Moreno-Cardenas, C. Arenillas, K. Bernatowicz, R. Comas, S. Li, D. P. Kodack, R. Fasani, A. Garcia, J. Gonzalo-Ruiz, A. Piris-Gimenez, P. Nuciforo, G. Kerr, R. Intini, A. Montagna, M. M. Germani, G. Randon, A. Vivancos, R. Smits, D. Graus, R. Perez-Lopez, C. Cremolini, S. Lonardi, F. Pietrantonio, R. Dienstmann, J. Tabernero, R. A. Toledo, RNF43 mutations predict response to anti-BRAF/EGFR combinatory therapies in BRAF(V600E) metastatic colorectal cancer. *Nat. Med.* **28**, 2162–2170 (2022).
51. S. Chen, Y. Zhao, S. Liu, J. Zhang, Y. G. Assaraf, W. Cui, L. Wang, Epigenetic enzyme mutations as mediators of anti-cancer drug resistance. *Drug Resist. Updat.* **61**, 100821 (2022).
52. M. L. Eich, M. Athar, J. E. Ferguson III, S. Varambally, EZH2-targeted therapies in cancer: Hype or a reality. *Cancer Res.* **80**, 5449–5458 (2020).
53. J. L. Anglin, Y. Song, A medicinal chemistry perspective for targeting histone H3 lysine-79 methyltransferase DOT1L. *J. Med. Chem.* **56**, 8972–8983 (2013).
54. M. H. Cho, J. H. Park, H. J. Choi, M. K. Park, H. Y. Won, Y. J. Park, C. H. Lee, S. H. Oh, Y. S. Song, H. S. Kim, Y. H. Oh, J. Y. Lee, G. Kong, DOT1L cooperates with the c-Myc-p300 complex to epigenetically derepress CDH1 transcription factors in breast cancer progression. *Nat. Commun.* **6**, 7821 (2015).
55. C. W. Chen, R. P. Koche, A. U. Sinha, A. J. Deshpande, N. Zhu, R. Eng, J. G. Doench, H. Xu, S. H. Chu, J. Qi, X. Wang, C. Delaney, K. M. Bernt, D. E. Root, W. C. Hahn, J. E. Bradner, S. A. Armstrong, DOT1L inhibits SIRT1-mediated epigenetic silencing to maintain leukemic gene expression in MLL-rearranged leukemia. *Nat. Med.* **21**, 335–343 (2015).
56. J. M. Benito, L. Godfrey, K. Kojima, L. Hogdal, M. Wunderlich, H. Geng, I. Marzo, K. G. Harutyunyan, L. Golfman, P. North, J. Kerry, E. Ballabio, T. N. Chonghaile, O. Gonzalo, Y. Qiu, I. Jeremias, L. Debose, E. O'Brien, H. Ma, P. Zhou, R. Jacamo, E. Park, K. R. Coombes, N. Zhang, D. A. Thomas, S. O'Brien, H. M. Kantarjian, J. D. Leverson, S. M. Kornblau, M. Andreeff, M. Muschen, P. A. Zweidler-McKay, J. C. Mulloy, A. Letai, T. A. Milne, M. Konopleva, MLL-rearranged acute lymphoblastic leukemias activate BCL-2 through H3K79 methylation and are sensitive to the BCL-2-specific antagonist ABT-199. *Cell Rep.* **13**, 2715–2727 (2015).
57. J. Han, Y. Liu, S. Yang, X. Wu, H. Li, Q. Wang, MEK inhibitors for the treatment of non-small cell lung cancer. *J. Hematol. Oncol.* **14**, 1 (2021).
58. L. Jin, J. Chun, C. Pan, D. Li, R. Lin, G. N. Alesi, X. Wang, H. B. Kang, L. Song, D. Wang, G. Zhang, J. Fan, T. J. Boggon, L. Zhou, J. Kowalski, C. K. Qu, C. E. Steuer, G. Z. Chen, N. F. Saba, L. H. Boise, T. K. Owonikoko, F. R. Khuri, K. R. Magliocca, D. M. Shin, S. Lonial, S. Kang, MAST1 drives cisplatin resistance in human cancers by rewiring cRaf-independent MEK activation. *Cancer Cell* **34**, 315–330.e7 (2018).
59. Y. Kobayashi, S. O. Lim, H. Yamaguchi, Oncogenic signaling pathways associated with immune evasion and resistance to immune checkpoint inhibitors in cancer. *Semin. Cancer Biol.* **65**, 51–64 (2020).
60. D. M. Gershenson, C. Gourley, J. Paul, MEK inhibitors for the treatment of low-grade serous ovarian cancer: Expanding therapeutic options for a rare ovarian cancer subtype. *J. Clin.* **38**, 3731–3734 (2020).
61. D. K. Mahapatra, V. Asati, S. K. Bharti, MEK inhibitors in oncology: A patent review (2015-present). *Expert Opin. Ther. Pat.* **27**, 887–906 (2017).
62. J. E. Chaft, A. Rimner, W. Weder, C. G. Azzoli, M. G. Kris, T. Cascone, Evolution of systemic therapy for stages I-III non-metastatic non-small-cell lung cancer. *Nat. Rev. Clin. Oncol.* **18**, 547–557 (2021).
63. J. J. Grob, Is there any interest in a new BRAF–MEK inhibitor combination in melanoma? *Lancet Oncol.* **19**, 580–581 (2018).
64. S. Kopetz, A. Grothey, R. Yaeger, E. Van Cutsem, J. Desai, T. Yoshino, H. Wasan, F. Ciardiello, F. Loupakis, Y. S. Hong, N. Steeghs, T. K. Guren, H. T. Arkenau, P. Garcia-Alfonso, P. Pfeiffer, S. Orlov, S. Lonardi, E. Elez, T. W. Kim, J. H. M. Schellens, C. Guo, A. Krishnan, J. Dekervel, V. Morris, A. Calvo Ferrandiz, L. S. Tarpgaard, M. Braun, A. Gollerkeri, C. Keir, K. Maharry, M. Pickard, J. Christy-Bittel, L. Anderson, V. Sandor, J. Tabernero, Encorafenib, binimetinib, and cetuximab in BRAF V600E–mutated colorectal cancer. *N. Engl. J. Med.* **381**, 1632–1643 (2019).
65. R. J. Sullivan, J. Weber, S. Patel, R. Dummer, M. S. Carlino, D. S. W. Tan, C. Lebbe, S. Siena, E. Elez, L. Wollenberg, M. D. Pickard, V. Sandor, P. A. Ascierto, A Phase Ib/II study of the BRAF inhibitor encorafenib plus the MEK inhibitor binimetinib in patients with BRAF(V600E/K) -mutant solid tumors. *Clin. Cancer Res.* **26**, 5102–5112 (2020).
66. Z. Liu, Y. Liu, L. Qian, S. Jiang, X. Gai, S. Ye, Y. Chen, X. Wang, L. Zhai, J. Xu, C. Pu, J. Li, F. He, M. Huang, M. Tan, A proteomic and phosphoproteomic landscape of KRAS mutant cancers identifies combination therapies. *Mol. Cell* **81**, 4076–4090.e8 (2021).

Acknowledgments

Funding: This work was supported by grants from the National Natural Science Foundation of China (nos. 82073320 to L.W., 81973365 to C.W., and 82173685 to X.Z.), the Central Guidance on Local Science and Technology Development Fund of Liaoning Province (no. 2022JH6/100100038 to W.C.), and the "Xingliao Talents" Program of Liaoning Province (no. XLYC1902008 to L.W.). **Author contributions:** L.W. conceived the study. J.Z., T.Y., Y.R., W.C., M.H., X.W., and N.G. acquired samples and performed the experiments and data analyses. W.Y., S.L., Y.Z., X.Z., L.J., J.Y., and C.W. analyzed and interpreted the data. J.Z. and L.W. wrote and revised the manuscript. All authors read and approved the final manuscript. **Competing interests:** The authors declare that they have no competing interests. **Data and materials availability:** All data needed to evaluate the conclusions in the paper are present in the paper and/or the Supplementary Materials.

Submitted 9 May 2022
Accepted 25 April 2023
Published 31 May 2023
10.1126/sciadv.adc9273